

Accepted Manuscript

Influence of temperature and pressure on the density and speed of sound of 2-hydroxyethylammonium propionate ionic liquid

João A. Sarabando, Paulo J.M. Magano, Abel G.M. Ferreira, Jaime B. Santos, Pedro J. Carvalho, Silvana Mattedi, I.M.A. Fonseca

PII: S0021-9614(18)30222-2
DOI: <https://doi.org/10.1016/j.jct.2018.03.016>
Reference: YJCHT 5361

To appear in: *J. Chem. Thermodynamics*

Received Date: 6 December 2017
Revised Date: 10 March 2018
Accepted Date: 20 March 2018

Please cite this article as: Joatildeo A. Sarabando, P.J.M. Magano, A.G.M. Ferreira, J.B. Santos, P.J. Carvalho, S. Mattedi, I.M.A. Fonseca, Influence of temperature and pressure on the density and speed of sound of 2-hydroxyethylammonium propionate ionic liquid, *J. Chem. Thermodynamics* (2018), doi: <https://doi.org/10.1016/j.jct.2018.03.016>

This is a PDF file of an unedited manuscript that has been accepted for publication. As a service to our customers we are providing this early version of the manuscript. The manuscript will undergo copyediting, typesetting, and review of the resulting proof before it is published in its final form. Please note that during the production process errors may be discovered which could affect the content, and all legal disclaimers that apply to the journal pertain.



Influence of temperature and pressure on the density and speed of sound of 2-hydroxyethylammonium propionate ionic liquid

João A. Sarabando^a, Paulo J. M. Magano^b, Abel G.M. Ferreira^{a,*}, Jaime B. Santos^b, Pedro J. Carvalho^c, Silvana Mattedi^d, I.M.A. Fonseca^a

^a GERST – Group on Environment, Reaction, Separation and Thermodynamics, Department of Chemical Engineering, University of Coimbra, Rua Sílvio Lima, 3030-790, Coimbra, Portugal

^b CEMMPRE, Department of Electrical and Computers Engineering, University of Coimbra, Polo II, Rua Sílvio Lima, 3030-970 Coimbra, Portugal

^c CICECO – Aveiro Institute of Materials, Department of Chemistry, University of Aveiro, 3810-193 Aveiro, Portugal

^d Escola Politécnica, Universidade Federal da Bahia, Rua Aristides Novis 2, Federação, 40210-630 Salvador, Bahia, Brazil

Keywords: 2- Hydroxyethylammonium propionate; Density; Speed of sound; GMA equation of state; Wu equation

* Corresponding author E-mail: abel@eq.uc.pt (Abel G. M. Ferreira)

Abstract

The alkanolammonium ILs are protic ionic liquids (PILs) with huge potential in a variety of industrial fields. Among other advantages, these PILs have low cost of preparation, simple synthesis and purification methodologies and low toxicity. This study aims at obtaining significant data on the fundamental thermophysical properties of hydroxyethylammonium-based PILs with carboxylate anions. The density was measured within the temperature and pressure intervals (298.15 to 343.15) K and (0.1 to 35.0) MPa for 2-hydroxyethylammonium propionate, [2-HEA][Pr]. The speed of sound was determined in the ranges (303.15 to 353.15) K and (0.1 to 20.0) MPa for the same substance. The estimated combined standard uncertainties are $\pm 0.45 \text{ kg}\cdot\text{m}^{-3}$ for density and $\pm 1.6 \text{ m}\cdot\text{s}^{-1}$ for speed of sound. The experimental pVT data were fitted using the Goharshadi–Morsali–Abbaspour equation of state (GMA EoS) with average relative absolute deviation (%AARD) of 0.03%. Thermomechanical coefficients as the thermal expansivity, isothermal compressibility, and internal pressure, were calculated using GMA EoS with the internal pressure being further compared with calculated values of cohesive energy density. The experimental pVT data were further successfully described by the predictive methods of Gardas and Coutinho and Paduszyński and Domańska.

1. Introduction

Ionic liquids (ILs) are salts with melting points below 100 °C, which can be divided into two main families, viz. aprotic ionic liquids (AILs) and protic ionic liquids (PILs). The PILs are synthesized by a proton transfer on stoichiometric acid-base Brønsted reaction. Compared to AILs, the main difference is the presence of at least a proton in PILs which is/are able to promote extensive hydrogen bonding [1]. Their protic nature boosted their increasing interest, by academia, as feasible candidates for a number of applications, including biological applications [2], organic synthesis [3-5], chromatography [6], as electrolytes for polymer membrane fuel cells [7], as reactants in biodiesel production [8], and as propellant or explosives [9,10]. Experimental studies for thermophysical properties of ILs have been reported for imidazolium-, pyridinium- and for some ammonium-based ILs, which are based in primary ammine cations of the form R_4N (R is an alkyl group). The alkanolammonium ILs are protic ionic liquids with a huge potential in a variety of industrial fields. Alkanolamines soaps, PILs formed by the reaction between an alkanolammonium and fatty acids, are currently used in the formulation of industrial and hand-cleaners, cosmetic creams, aerosols and shave foams due to their emulsifier, and detergent ability in oil-in-water emulsions [11-14]. The monoethanolamine oleate is widely used in the pharmaceutical industry as sclerosant agent [15-18]. Among other advantages, alkanolammonium PILs have low cost of preparation, and they are of simple synthesis and purification [19,20] as well as of low toxicity compared with other ILs [21,22]. Despite the well recognized fundamental and practical significance, their fundamental thermophysical properties are either scarce or absent. The density and the viscosity were measured by Kurnia *et al.* [19] for hydroxyethylammonium and bis-(hydroxyethyl)ammonium cations with acetate and lactate anions. The only study of the hydroxyethylammonium propionate density was made at atmospheric pressure by Kurnia *et al.* [23]. Iglesias *et al.* [20] further evaluated the speed of sound and electrical conductivity, at atmospheric pressure, for the 2-hydroxyethylammonium, bis(2-hydroxyethyl)ammonium, and tris(2-hydroxyethyl)ammonium cations with the pentanoate anion. Experimental data on density, viscosity,

speed of sound and refractive index as well as IR and NMR spectra were reported by Alvarez *et al.* [24] for the N-methyl-2-hydroxyethylammonium cation with various carboxylates (formate, acetate, propionate, butyrate, isobutyrate and pentanoate). Pinkert *et al.* [25], presented density, viscosity and electrical conductivity data for the 2-hydroxyethylammonium, 3-hydroxypropylammonium, bis(2-hydroxyethyl)ammonium, and tris(2-hydroxyethyl)ammonium cations combined with formate, acetate and malonate anions.

This study aims at obtaining significant data, on a wide temperature and pressure ranges, for the density and the speed of sound of 2-hydroxyethylammonium propionate [2-HEA][Pr], following previous work on ethanolammonium-based PILs with common cation N-methyl-2-hydroxyethylammonium [m-2-HEA] and anions propionate [Pr], butanoate [Bu] and pentanoate [Pe], [26-28]. The density and its pressure-temperature dependency (pVT behaviour) can be considered as fundamental data for developing equations of state, which are one of the main tools used for thermophysical properties prediction for process design purposes, and solution theories of ILs. Moreover the derived properties from density as the thermomechanical coefficients (thermal expansivity, isothermal compressibility, and internal pressure) provide useful information on IL structure and molecular interactions. The volumetric behaviour of ILs are described here in terms of the Goharshadi–Morsali–Abbaspour equation of state (GMA EoS), which has been developed and found to be valid for polar, non-polar, and H-bonded fluids [29]. The experimental pVT data of the PILs were successfully described by the predictive methods of Gardas and Coutinho [30] and Paduszyński and Domańska [31].

The speed of sound for ILs is, compared to density, a forgotten property. From 2010, the IL Thermo database [32] records 242 ILs studied, distributed by imidazolium (51%), pyridinium (16%), pyrrolidinium (9%), ammonium (22%) and phosphonium (2%). The hydroxyethylammoniums contribute with 5% (23% of the ammoniums studied). The speed of sound has been reported for the methylhydroxyethylammonium [24] and 2-hydroxyethylammonium with carboxylate anions only by

Iglesias and co-workers [20,33,34]. To our knowledge the speed of sound of 2-hydroxyethylammonium propionate is here reported for the first time. The predictive model for speed of sound, based on a corresponding states group contribution method, proposed by Wu *et al.* [35] is here evaluated.

2. Experimental

2.1. Chemicals

The 2-hydroxyethylammonium propionate, [2-HEA][Pr], was prepared from stoichiometric quantities of the ethanolamine with propanoic acid using the methodology described in detail by Talavera-Prieto *et al.* [26]. The PIL was dried under vacuum (1 Pa) and the distilled, water and volatile-rich was discarded. Thereafter, it was distilled under high vacuum (*ca.* 100 Pa) and the purity of the distillate checked by ^1H NMR and ^{13}C NMR using dimethylsulfoxide (DMSO) as a solvent (see Figures S1 and S2 in Supporting Information). The NMR spectra, and the peak integration, show clearly the correct stoichiometry and the high purity of the synthesized compound. Note that only the ^1H NMR is quantitative and thus, useful to evaluate the compound's purity; the purity was found to be greater than 98% with water content lower than 100 ppm. The IL water content was determined with a Metrohm 831 Karl Fisher.

The chemical structure, compound description, CAS number, water mass fraction designation, mass fraction purity and supplier, of the IL and calibration liquids are reported in Table 1. The water used was HPLC (high performance Liquid Chromatography / Scharlau) (indicated by its electrical conductivity of $1\mu\text{S} \cdot \text{cm}^{-1}$). The toluene used was of analytical quality, also to mass fraction purity, 0.9999 (w / w).

Table 1

2.2. Measurements

The experimental densities, ρ , were measured using the Anton Paar DMA 60 digital vibrating-tube densimeter, with a DMA 512P measuring cell, within the temperature range of 298.15 K to 343.15 K and pressure interval (0.1 to 35.0) MPa. The installation of the DMA measurement system including the peripheral equipment was described in detail in a previous work [26]. The temperature in the vibrating-tube cell was measured with a platinum resistance probe with an uncertainty of ± 0.01 K. The probe was previously calibrated in the (273.15–373.15) K temperature range against a platinum resistance thermometer ERTCOEutechnics High Precision Digital Thermometer certified in the ITS90. A Julabo P-5 thermostatic bath, with silicone oil as circulating fluid, was used in the thermostat circuit of the measuring cell with a stability and accuracy of 0.01 K. The required pressure was generated and controlled with a Pressure Generator model 50-6-15 High Pressure Co. Pressure was measured with a pressure transducer (Wika Transmitter S-10) with a maximum uncertainty of ± 0.03 MPa. A NI PCI-6220 data acquisition board (DAQ), from National Instruments, was used for the real-time registration of the period, temperature, and pressure values. Temperature (NI SCC-FT01) and pressure (NI SCC-CI20) modules were installed in a NI SC-2345 shielded carrier and connected to the DAQ board in order to monitor the signals. Water and toluene were used as reference fluids to fit the calibration equation proposed by Lampreia and Nieto de Castro [36]. The combined standard uncertainty of the density measurements was found to be $u_c(\rho) = \pm 0.45 \text{ kg}\cdot\text{m}^{-3}$, which was estimated taking into account the influence of uncertainties associated with the calibration equation, temperature, period of oscillations (six-digit frequency counter), viscosity, and density data of calibrating fluids. The combined expanded uncertainty with a 95% confidence level (coverage factor $k = 2$) was estimated to be $U_c(\rho) = 0.90 \text{ kg}\cdot\text{m}^{-3}$.

A stainless steel cell designed for liquid speed of sound, u , measurements was used and is fully described in a previous study [37]. The instrumentation and procedure used in this work were revised according to the schematic representation shown in Figure 1.

Figure 1

Two 5 MHz ultrasonic transducers (one acting as an emitter and the other as a receiver) were mounted in cavities drilled on a stainless steel block. The ultrasound wave, corresponding to the path between the transmitter and receiver, was collected by a NI-PCI data acquisition board and recorded by means of a computer program. The developed Labview program allows an easy wave propagation time calculation, in the liquid, which is obtained subtracting the time that the acoustical wave takes to travel between the emitter and receiver from the propagation time in the cell steel walls.

The system temperature was controlled, by means of a flexible silicone resistance cable wrapped around the cell, using an electronic thermostat (Red Line Series RD31) whose temperature probe is inserted in the resistance coil. The experimental setup was placed in a thermal insulation glove box, to avoid heat losses, and is able to maintain the temperature within *ca.* ± 0.1 K. The temperature was measured using an external digital thermometer by isothermal Technology (ISOTECH TTI-10), with a precision of 0.01 K, placed directly in a cavity of the cell and close to the sample. The pressure was measured using a manometer by Keller (Mano 2000 LEO 2), with an accuracy of ± 0.02 MPa.

The cell was calibrated by measuring the speed of sound in water [38] and toluene [38], for the overall temperature and pressure ranges (298.15 - 348.15) K, and (0.1-20) MPa using a total of 156 data points. The following calibration equation, from Gomes de Azevedo and co-workers' work [39], was adopted as the calibration curve:

$$\frac{1}{u} = C_1 + C_2T + C_3T^2 + (C_4 + C_5T + C_6T^2)p + [C_7 + C_8T + C_9T^2 + (C_{10} + C_{11}T + C_{12}T^2)p]\Delta t \quad (1)$$

where C_1 - C_{12} are calibration constants, p is the pressure (MPa) and Δt (μs) is the wave propagation time in the IL. The values of calibration constants and statistical indicators of calibration Eq. (1) are listed in Table 2. Eq. (1) gives a very good representation of the calibrants (u, T, p) speed of sound data as shown by the very low standard deviation relative to speed of sound (σ_u) and average absolute relative deviation ($\%AARD_u$). These quantities were defined as:

$$\sigma_u = \left[\sum_{i=1}^N (u_{cal} - u)_i^2 / (N - 12) \right]^{1/2} \quad (2)$$

$$\%AARD_u = \frac{100}{N} \times \sum_{i=1}^N \left| \frac{u_{calc} - u}{u} \right|_i \quad (3)$$

where N is the number of data points, u_{calc} is the calculated value of speed of sound with Eq. (1) and u is the reported experimental value at the same temperature (and pressure) of corresponding point i . The application of the law of propagation of uncertainty to Eq. (1), taking in consideration the temperature, pressure, period of oscillations, and the calibrating fluids speed of sound uncertainties, allows to determine the speed of sound combined standard uncertainty to be $u_c(u) = \pm 1.6 \text{ m}\cdot\text{s}^{-1}$.

Table 2

3. Results and discussion

The density measurements for [2-HEA][Pr] have been carried out in the broad range of temperatures $T = (293.15 \text{ to } 343.15) \text{ K}$ and pressures $p = (0.1 \text{ to } 35.0) \text{ MPa}$. Table 3 and Figure 2 report the density behaviour as function of pressure and temperature.

Table 3

Figure 2 about here

A comparison against literature data reported by Kurnia *et al.* [23], at temperatures in the range $T = (293.15 \text{ to } 313.15) \text{ K}$ and at atmospheric pressure, is presented in Figure 3. The authors used a digital vibrating glass U-tube densimeter (DMA 5000, Anton-Paar), calibrated using Millipore quality water and dry air according to the established standard procedures [23], with a combined standard uncertainty of $3 \times 10^{-3} \text{ kg} \cdot \text{m}^{-3}$. As depicted, the density data of Kurnia *et al.* presents some significant deviations for lower temperatures but they are crossing our values for higher temperatures: the relative deviations between the two sets of data are of 1% at 298.15 K and decrease to 0.4% at 313.15 K.

Figure 3

The GMA EoS was used to correlate the density data. The GMA EoS is given as [29]:

$$(2z-1)V_m^3 = A(T) + B(T) \rho_m \quad (4)$$

where z , V_m , and ρ_m are the compressibility factor, molar volume, and molar density, respectively. Under isothermal conditions, the quantity $(2z-1)V_m^3$, as a function of molar density, presents a linear behaviour and the fitting of these two quantities allows to determine $A(T)$, through the intercept, and $B(T)$, through the slope. The temperature dependencies of the parameters $A(T)$ and $B(T)$ are given by the equations [29]:

$$A(T) = A_0 - \frac{2A_1}{RT} + \frac{2A_2 \ln T}{R} \quad (5)$$

$$B(T) = B_0 - \frac{2B_1}{RT} + \frac{2B_2 \ln T}{R} \quad (6)$$

where A_0 - A_2 and B_0 - B_2 are fitting parameters, and R is the gas constant. The parameters were calculated by least squares fitting of Eq. (4) to density data. Table 4 contains the coefficients A_0 - A_2 and B_0 - B_2 , and statistical indicators.

Table 4

As depicted in Figure 4, an excellent agreement between experimental data and analytical behaviour of GMA EoS is observed, with the term $(2z-1)V_m^3$ showing a linear dependency with the molar density. Thus, GMA EoS stands as a very reliable equation of state to describe/calculate the density of [2-HEA][Pr] within the studied temperature and pressure ranges, with standard deviation in density similar to that inherent to the experimental determination. The absolute differences in density $|\rho_{\text{exp}}-\rho_{\text{cal}}|$ are lower than $0.3 \text{ kg}\cdot\text{m}^{-3}$.

Figure 4

The density of the liquid at a given (T, p) state was calculated from:

$$B(T)\rho_m^5 + A(T)\rho_m^4 + \rho_m - 2p/RT = 0 \quad (7)$$

which results by solving Eq. (4) for ρ_m . The predictive ability of the GMA EoS to reproduce experimental data was evaluated by calculating the relative percentage deviation ($\%RD_\rho$) between predicted and experimental values of densities using Eq. (8) and the corresponding $\%AARD_\rho$ calculated through Eq. (9):

$$\%RD_\rho = 100 \times \frac{\rho_{\text{calc}} - \rho}{\rho} \quad (8)$$

$$\%AARD_\rho = \frac{100}{N} \times \sum_{i=1}^N \left| \frac{\rho_{\text{calc}} - \rho}{\rho} \right| \quad (9)$$

where N is the number of data points, ρ_{calc} is the calculated value of density with GMAEoS and ρ is the reported experimental value at the same temperature (and pressure). As depicted in Figure 5, the relative deviations between values calculated by the GMA EoS and the experimental data, as a function of temperature and pressure, are very small, ranging within $\pm 0.05 \%$.

Figure 5

Some important thermomechanical properties, like the thermal expansivity, $\alpha_p = - (1/\rho)(\partial\rho/\partial T)_p$, and isothermal compressibility $k_T = (1/\rho)(\partial\rho/\partial p)_T$, can be derived from the GMA equation of state as follows [40]:

$$\alpha_p = \frac{(2B_1 + 2B_2T)\rho_m^5 + (2A_1 + 2A_2T)\rho_m^4 + 2p}{5\rho_m^5(RT^2B_0 - 2B_1T + 2B_2T^2 \ln T) + 4\rho_m^4(RT^2A_0 - 2A_1T + 2A_2T^2 \ln T) + RT^2\rho_m} \quad (10)$$

$$k_T = \frac{2}{\rho_m RT + 5\rho_m^5(RTB_0 - 2B_1 + 2B_2T \ln T) + 4\rho_m^4(RTA_0 - 2A_1 + 2A_2T \ln T)} \quad (11)$$

The density variations over isothermal or isobaric paths are usually smooth functions of temperature and pressure. However, the mechanical coefficients are quite sensitive to subtle changes in the density. The calculated mechanical coefficients from GMA EoS, α_p and k_T , are presented in Table S1 of the Supplementary Information. Figure 6 shows the behaviour of α_p as function of temperature and pressure. The expected behaviour is observed, *i.e.* α_p decreases with the increase of pressure, at isothermal conditions and increases with the temperature, at fixed pressures. The minimum and maximum α_p found, in the studied ranges of temperature and pressure, are $7.81 \times 10^{-4} \text{ K}^{-1}$ for (298.15 K, 35 MPa) and $13.75 \times 10^{-4} \text{ K}^{-1}$ at (343.15 K, 0.1 MPa) respectively. At 298.15 K and 0.1 MPa, $\alpha_p = 8.97 \times 10^{-4} \text{ K}^{-1}$. These values are higher than those calculated, with the same method, for [m-2-HEA][Pr] in our previous work [26], denoting slightly higher intermolecular interactions of the [2-HEA][Pr], compared to those of [m-2-HEA][Pr].

Figure 6

The isothermal compressibility is represented Figure 7 as a function of temperature and pressure. As observed, k_T increases with temperature under at isobaric conditions. It decreases with pressure at fixed temperatures. The minimum and maximum values obtained are 0.261 GPa^{-1} (at 298.15 K, 35 MPa) and 0.520 GPa^{-1} (at 343.15 K, 0.1 MPa), respectively. At 298.15 K and 0.1 MPa, $k_T = 0.285 \text{ GPa}^{-1}$.

Figure 7

The thermal pressure coefficient, γ_V , can be calculated according to $\gamma_V = \alpha_p / k_T$. On the basis of the thermomechanical coefficients, the internal pressure p_i can be calculated according to:

$$p_i = (\partial U / \partial V)_T = T (\partial p / \partial T)_V - p = T \cdot \gamma_V - p \quad (12)$$

where U is the internal energy. Although rarely used in the ionic liquids investigation, the internal pressure provides a useful basis for understanding the nature of molecular interactions in the liquid state. As the internal pressure is related to the isothermal change of entropy per unit volume it is a macroscopic property used for estimating the cohesion of liquids reflecting molecular order. The internal pressure is a measure of the change in internal energy of a liquid as it experiences a small isothermal expansion. The interactions most affected by such a small change in volume include repulsion, dispersion, and weak dipolar interactions and for non-electrolyte liquids in which these effects are important, the values of p_i approach those of cohesive pressure [41,42]. Cohesive pressure or cohesive energy density, CED , is defined as the ratio between the cohesive energy, U_c , and the molar volume, V_m . Cohesive energy can be obtained from the enthalpy of vaporization, $\Delta_{\text{vap}}H$, as:

$$U_c = \Delta_{\text{vap}}H - RT \quad (13)$$

Reid *et al.* [43] found that ammonium PILs (acetate family) can vaporize as their neutral acid and base precursors and they found a strong correlation between the enthalpy of vaporization, $\Delta_{\text{vap}}H_m^0(\text{PIL})$, at 298.15 K and atmospheric pressure, and the corresponding values of the precursor amine, $\Delta_{\text{vap}}H_m^0(\text{amine})$:

$$\Delta_{\text{vap}}H_m^0(\text{PIL}) = (0.968 \pm 0.145) \Delta_{\text{vap}}H_m^0(\text{amine}) + (74.1 \pm 6.1) \quad (14)$$

For acetic and propionic acids the reported $\Delta_{\text{vap}}H_m^0$ are $51.6 \text{ kJ}\cdot\text{mol}^{-1}$ [44] and $51.0 \text{ kJ}\cdot\text{mol}^{-1}$ [45] respectively. Thus, in a good approximation, the values of $\Delta_{\text{vap}}H_m^0(\text{PIL})$ derived for acetate PILs can be considered as the same for propionate ones. For ethanolamine $\Delta_{\text{vap}}H_m^0(\text{amine}) = 58 \text{ kJ}\cdot\text{mol}^{-1}$ [45] and from Eq. (14), $\Delta_{\text{vap}}H_m^0(\text{PIL}) = 130.244 \text{ kJ}\cdot\text{mol}^{-1}$ which gives $CED = 1060 \text{ MPa}$ for [2-HEA][Pr].

The values of the internal pressure of [2-HEA][Pr] are given as function of temperature at $p = 0.1 \text{ MPa}$ in Figure 8. In the same figure the value the cohesive pressure at 298.15 K is also represented.

Figure 8

Kartsev and co-workers [46,47] have made studies on molecular fluids including polar, non-polar and associated solvents and concluded that, at atmospheric pressure, systems with temperature coefficients greater than zero, $(\partial p_i / \partial T) > 0$, lead to hydrogen-bonded structures in the liquid, while $(\partial p_i / \partial T) < 0$ translates on lower association of species. To the best of our knowledge, for ILs no such study has been performed before. The [2-HEA][Pr] can have cation-cation (CC) and cation-anion (CA) $\text{O}\cdots\text{H}\cdots\text{H}$ hydrogen bonding. The CA interaction can be further divided into subcategories N-H \cdots O-C (between ammonium hydrogen and carboxylate oxygen) and O-H \cdots O-C (between hydroxyl group and carboxylate oxygen). Thummuru and Mallik [48] performed molecular dynamics simulations of hydrogen bonding in hydroxyl-functionalized protic ammonium carboxylate PILs which included the 2-hydroxyethylammonium acetate [2-HEA][Ac] among others. Thummuru and Mallik [48] reported that the inclusion of (OH) group decrease the CA interactions compared to when it is absent from the cation, and it increases also the solvation shell of the PIL and thus the long-range interactions. As two types of acidic hydrogen atoms are present in the cation (hydroxyl and ammonium groups) the anionic density must spread around these two type of atoms on the cation. However, proeminence of carboxylate density around the ammonium hydrogens was reported [48]. These conclusions, will most likely be

valid for [2-HEA][Pr]. From Figure 8 a general weak dependence of p_i on temperature is observed at low and high pressure with a clear change in the sign of $(\partial p_i / \partial T)$ observed near 313 K which probably means some changes in the association structure of [2-HEA][Pr]. As indicated by Ivanov and Abrosimov [49] for molecular fluids, the existence of intermolecular hydrogen bonding in a liquid substantially increases the CED relative to p_i . This behaviour is also observed in Figure 8 for [2-HEA][Pr]. Then we can conclude that hydrogen-bonding must play an important role in the structure of liquid [2-HEA][Pr]. It has been considered that the relationship $p_i = n \cdot CED$ holds [50]. The CED have been calculated for some imidazolium, pyridinium and pyrrolidinium ILs [50] but values for ammonium PILs are lacking. For [2-HEA][Pr] at 298.15 K $n=0.89$ which is higher than the values found for imidazolium, pyridinium and pyrrolidinium ILs for which $0.56 < n < 0.87$ [50].

The group contribution methods (GCM) proposed by Gardas and Coutinho [30] (GC GCM) and by Padaszyński and Domańska [31] (PD GCM) were used to predict the pVT data of [2-HEA][Pr]. The GC GCM method uses the volumes of ions at the reference temperature (298.15 K) and pressure (0.1 MPa). Ionic volumes can be calculated by means of the Ye and Shreeve procedure [51] or, if available, taken directly from the literature. The linear sum of the volumes of cation (V_+) and anion (V_-) is assumed [30]. The influence of temperature and pressure on the molar volume is accounted for by three universal (i.e., independent of IL) coefficients found by fitting the model equation to experimental density data. The authors assumed linear dependence of molar volume on temperature and pressure. The database used to obtain the coefficients included 1500 experimental density data points for 23 ILs covering the temperature and pressure ranges of $T = (293-393)$ K and $p = (0.1 \text{ to } 100)$ MPa. The %AARD between calculated and experimental densities ranges from 0.45% to 1.57% depending on the cation of IL (imidazolium, pyridinium, pyrrolidinium, or phosphonium) [30]. The density at coordinates (T, p) is given by [30]:

$$\rho(T, p) = \frac{M}{N(V_+ + V_-)(0.8005 + 6.652 \cdot 10^{-4}T - 5.919 \cdot 10^{-4}p)} \quad (15)$$

where ρ is the density, M is the IL molar mass, N is the Avogadro number, T is the temperature, and p (MPa) is the pressure.

The (PD GCM) method is based on the Tait equation, in which the molar volume at reference temperature (298.15 K) and pressure (0.1 MPa) was assumed to be additive with respect to a defined set of both cationic and anionic functional groups. PD GCM was developed based on a database containing over 18,500 data points for a variety of 1028 ILs covering a wide temperature and pressure ranges of $T = (253 \text{ to } 473) \text{ K}$ and $p = (0.1 \text{ to } 300) \text{ MPa}$. The PD GCM model parameters, including contributions to molar volume of 177 functional groups, as well as universal coefficients, describing the PVT surface, were fitted to experimental data of 828 ILs with an %AARD = 0.53% [31]. The model was evaluated against a test set of 200 ILs, not included in the development of the correlation, showing an %AARD = 0.45%. The density of the IL for the reference temperature and pressure conditions $\rho_0 = \rho (T_0 = 298.15 \text{ K}, p_0 = 0.1 \text{ MPa})$ was given by the following formula [31]:

$$\rho_0 = \rho(T_0, p_0) = \frac{M}{V_{0,m}} \quad (16)$$

where M is the molar mass of the IL and $V_{0,m}$ is the molar volume at (T_0, p_0) which is calculated based on the GCM additivity principle:

$$V_{0,m} = \sum_i n_i v_i^0 \quad (17)$$

Parameters n_i and v_i^0 correspond to the number of functional group occurrences of type i , and the contribution of that group to molar volume at (T_0, p_0) , respectively. In that model, the relationship [31]:

$$\rho(T, p_0) = \left[\frac{\rho_0}{1 + 6.439 \cdot 10^{-4} (T - T_0)} \right] \quad (18)$$

is combined with the Tait-type equation for compressed fluid:

$$\rho(T, p) = \frac{\rho(T, p_0)}{1 - 0.081 \ln[1 + B(T)(p - p_0)]} \quad (19)$$

where

$$B(T) = \frac{1}{195} [1 + 4.97 \cdot 10^{-3} (T - T_0)] \quad (20)$$

ILs with the common 2-hydroxyethylammonium cation combined with various carboxylic acid anions were considered in the PD GCM model [31]: ammonium-based cations containing the hydroxyethyl group ($-C_2OH$) include 2-hydroxyethylammonium, bis(2-hydroxyethyl) ammonium, tris(2-hydroxyethyl)ammonium, and the formate, acetate, and pentanoate anions. Paduszyński and Domanska [31] made predictions of densities of those ILs over a 60 K range near the ambient temperature and at $p = 0.1$ MPa and with average absolute relative deviations ranging from $\pm 0.2\%$ to $\pm 2.5\%$.

For the application of GC GCM the molecular volumes of ions $V[2\text{-HEA}]$ and $V[\text{Pr}]$ are needed. The molecular volumes of carboxylic ammonium PILs have been proposed in our previous work [26], by fitting Eq. (15) to the experimental density data of the PILs. In that work we have found $V[m\text{-2-HEA}] = 11.75 \times 10^{-29} \text{ m}^3$ and $V[\text{Pr}] = 11.52 \times 10^{-29} \text{ m}^3$. Taking into account the contribution $V(-CH_3) = 3.0 \times 10^{-29} \text{ m}^3$ for the methyl group [50], it is obtained $V[2\text{-HEA}] = 8.75 \times 10^{-29} \text{ m}^3$ and Eq. (15) can be applied to predict density data of $[2\text{-HEA}][\text{Pr}]$. The density deviations between calculated and experimental values are plotted in Figure 9a as function of pressure and temperature. It is observed that %RDs are usually in the range $\pm 1\%$ and %AARD = 0.6% which allows to conclude that Eq. (15) gives a good prediction of data.

The group assignments for $[2\text{-HEA}][\text{Pr}]$ i.e., the n_i values and the group contributions necessary for application of PD GCM are presented in Table S2 given in Supplementary Information. The density deviations between the predicted values with PD GCM and the experimental values for $[2\text{-HEA}][\text{Pr}]$ in the given ranges of pressure and temperature can be seen in Figure 9b. It is observed that %RDs are always negative with maximum values around -2.5% , similar to what could be expected from the application of the method. The %AARD = 1.7% which can be considered as representative of a reasonable accuracy for the predictions.

Figure 9

The speed of sound measurements have been carried out for [2-HEA][Pr] over the range of temperatures $T=$ (303.15 to 353.15) K and pressures $p=$ (0.1 to 20.0) MPa. The experimental data are presented in Table 5 and Figure 10. To the best of our knowledge, speed of sound measurements for [2-HEA][Pr] are here reported for the first time.

Our original data have been fitted against temperature and pressure following the rational equation:

$$u = \frac{a_0 + a_1T + a_2T^2 + b_1p}{1 + a_3T + b_2p} \quad (21)$$

where a_0 - a_2 and b_1 and b_2 are the fitting parameters. These parameters, calculated by least squares fitting of Eq. (21) to the sound speed experimental data, are presented in Table 6 were the usual statistical indicators were also included to show the ability of Eq. (21) to represent experimental data.

Table 5**Table 6****Figure 10**

As depicted in Figure 11, where the %RDs between calculated values from Eq. (21) and experimental data are represented, one can concluded that Eq. (21) gives a very reliable correlation of the sound speed of [2-HEA][Pr] for the studied ranges of temperatures and pressures : %AARD_u is 0.09% and the standard deviation is 1.7 m□s⁻¹. It was verified that about 70% of the values present deviations ($u-u_{cal}$) lower than σ_u : the maximum deviation obtained was ($u-u_{cal}$)= 3.54 m·s⁻¹ at the coordinates $T=323.15$, $p= 0.1$ MPa; the minimum deviation was -0.032 m·s⁻¹ at $T=343.15$ K, $p= 19$ MPa. From Figure 11, we conclude that the deviations are small, usually in the range of 0.09%. At atmospheric pressure, the RD% are within ±0.2 % corresponding to a mean deviation of ± 1.6 m·s⁻¹.

Figure 11

In Figure 12 the measured speed of sound as a function of temperature, at atmospheric pressure, is presented for ionic liquids with the common [2-HEA] cation combined with different carboxylic acid anions, like formate [F], acetate [Ac], propionate [Pr] and pentanoate [Pe]. The speed of sound data reported by Cota *et al.* [34], for [2-HEA][F], by Alvarez *et al.* [33], for [2-HEA][Ac], and by Iglesias *et al.* [20], for [2-HEA][Pe], are presented in Figure 12.

Fig 12.

As depicted, some discrepancies can be found: [2-HEA][Pr] speed of sound reported here presents similar values to those reported for the [2-HEA][Pe] [20]. Analyzing the property tendency as function of the carboxylate anion change, i. e. considering the positions relative to the acetate and pentanoate anions, one may infer that [2-HEA][Pr] data may present some inconsistency. However, it is surprising that measurements made for other [2-HEA]-based ILs, the smallest anion, are located between those of the acetate and pentanoate, thus breaking the trend of increasing the anion chain. The possible source of the above mentioned "out of place" discrepancies could be due to some water contamination of samples. Alvarez *et al.* [33] refer that [2-HEA][Ac] used in their experiments was dried for 48 h at room temperature under a vacuum of 20 kPa while stirring, before each use in order to decrease the water content as much as possible. For [2-HEA][F] and [2-HEA][Pe] authors did not provide relevant information on purity of PILs. The [2-HEA][Pr] samples used in this work were extensively purified as explained before (section 2.1).

Recently, Wu *et al.* proposed a corresponding states group contribution method for estimating the speed of sound of ILs at atmospheric pressure [35]:

$$u = \sum_{i=0}^3 a_i \left(\sum_{j=1}^k n_j \Delta u_{0,j} \right)^i (1 - T/T_c)^{0.65359} \quad (22)$$

where n_j is the number of groups of type j , k is the total number of different groups in the ionic fragments, and a_i and $\Delta u_{0,j}$ are parameters and group contribution parameters for group j , respectively. The critical temperature, T_c , is determined by Valderrama group of contribution method [52]:

$$T_c = \frac{T_b}{\left[0.5703 + 1.0121 \sum_{j=1}^k n_j \Delta T_{c,j} - \left(\sum_{j=1}^k n_j \Delta T_{c,j} \right)^2 \right]} \quad (23)$$

where n_j and $\Delta T_{c,j}$ are the number of occurrences and the contribution to the critical temperature of group j in the ionic species, respectively, k is the total number of different groups in the ionic fragment, and T_b is the predicted normal boiling point [52]:

$$T_b = 198.2 + \sum_{j=1}^k n_j \Delta T_{b,j} \quad (24)$$

where $\Delta T_{b,j}$ is the contribution to the normal boiling temperature of group j in the ionic species. Eq. (19) was based on speed of sound data of 96 pure ILs (containing 51 cations and 23 anions) reported between 2005 and 2013. An %AARD= 2.34% has been stated for the corresponding states group contribution method proposed by the authors for the 96 ionic liquids based on imidazolium, pyridinium, pyrrolidinium, phosphonium, and ammonium cations combined with a large variety of anions. For [2-HEA][Pr], $T_b = 537.63$ K and $T_c = 721.19$ K were obtained. The group assignments and the group contributions for the calculation of T_b and T_c of [2-HEA][Pr] with Valderrama method [52] as well as the same data for application of Wu method are presented in Table S3 given in supplementary data. In Figure 12, Values of the speed of sound using Eq. (22) are compared with those reported in this work. It can be concluded that the sound speeds predicted with Wu *et al.* equation [35] are always higher than the experimental values, with %RDs ranging between 7% and 10%, resulting in a %AARD of 7.9%. From Figure 12, looking at the (u, T) data for [2-HEA][Pr] predicted from Wu method, it can be concluded that they are correctly positioned between the corresponding data for [2-HEA][Ac] and [2-HEA][Pe]. However, this can not be taken for granted because Wu *et al.* [35] used data of those PILs for the training set from which the parameters of Eq. (22) were obtained. Wu *et al.* [35] referred that the

method could have some limitations for protic ILs due to the presence of proton-donor and proton-acceptor sites. Another criticism that can be made to Wu method is that its accuracy depends on the calculation of the critical temperature obtained by Valderrama method.

The fluid's sound speed, its density and isentropic compressibility (inverse bulk modulus), are essential properties to EoSs, models and correlations, which are related with each other as well as with the heat capacities at constant pressure and volume. The measured densities and sound speeds can be combined through Newton-Laplace equation, Eq. (25), to calculate the isentropic compressibility of [2-HEA][Pr] as presented in the Supporting Information in Table S4 and Figure 13:

$$k_s = \frac{1}{\rho u^2} \quad (25)$$

As depicted in Figure 13, k_s presents the common behaviour observed for ionic liquids, with T and p that in turn is related to the corresponding behaviour of density and speed of sound: k_s increases with temperature at isobaric conditions and decreases with pressure at isothermal conditions. The minimum and maximum values observed within the temperature (303.15 to 343.15) K and pressure (0.1 to 20) MPa range are $4.51 \times 10^{-11} \text{ Pa}^{-1}$ (at 303.15 K, 20 MPa) and $6.04 \times 10^{-11} \text{ Pa}^{-1}$ (at 343.15 K, 0.1 MPa), respectively. At 298.15 K and 0.1 MPa, $k_s = 4.90 \times 10^{-11} \text{ Pa}^{-1}$.

Figure 13

An important parameter in the study of liquid state is the molar compressibility, also called Wada's constant, [53] defined by:

$$k_m = \frac{M}{\rho} k_s^{-1/7} \quad (26)$$

The molar compressibility of [2-HEA][Pr], calculated from experimental densities and speeds of sound, was determined in the ranges $T = (303.15 \text{ to } 343.15) \text{ K}$ and $p = (0.1 \text{ to } 20) \text{ MPa}$ and are presented in Table 7. It is clearly observed that k_m is almost constant as function of temperature and pressure. As

the molar compressibility presents a small temperature and pressure dependency, the mean value $\langle k_m \rangle$ was determined as:

$$\langle k_m \rangle = (1/N) \sum_i^N (k_m)_i \quad (27)$$

over the range of pressure variation $(\langle k_m \rangle, p)_T$ for each isotherm and over the temperature variation $(\langle k_m \rangle, T)_p$ at each pressure. The corresponding standard deviation from the mean values for each isotherm or isobar was calculated as:

$$\sigma_{km} = \left[\sum_{i=1}^N (k_m - \langle k_m \rangle)_i^2 / N \right]^{1/2} \quad (28)$$

From the values $(\langle k_m \rangle, p)_T$ and $(\langle k_m \rangle, T)_p$ the overall means values were calculated giving $\langle k_m \rangle = (3.635 \pm 0.011) \times 10^{-3} / (\text{m}^3 \cdot \text{mol}^{-1} \cdot \text{Pa}^{1/7})$ and $\langle k_m \rangle = (3.635 \pm 0.026) \times 10^{-3} / (\text{m}^3 \cdot \text{mol}^{-1} \cdot \text{Pa}^{1/7})$, respectively. This value can be compared with $\langle k_m \rangle = (3.138 \pm 0.002) \times 10^{-3} / (\text{m}^3 \cdot \text{mol}^{-1} \cdot \text{Pa}^{1/7})$ obtained previously by us for N-methyl-2-hydroxyethylammonium propionate at $T = (298.15 \text{ to } 333.15) \text{ K}$ and atmospheric pressure [27]. The $\langle k_m \rangle$ can be considered as an appropriate and useful parameter characteristic of the IL over a broad range of pressures and temperatures. For example Eq. (26) can be solved for the speed of sound using Eq. (25) and assuming that $k_m = \langle k_m \rangle$:

$$u = \left(\frac{\langle k_m \rangle}{M} \right)^{7/2} \rho^3 \quad (29)$$

Thus, the speed of sound can be estimated at any desired temperature and pressure from density. For [2-HEA][Pr] the speed of sound predicted in this way gives %AARD = 2.4% a value which is much less than the corresponding value of 7.9 % obtained for the application of Wu method [35].

Table 7

4. Conclusions

The density of 2-hydroxyethylammonium propionate was measured in the $T=$ (293.15 to 343.15) K temperature range and for pressures ranging from atmospheric to 35.0. MPa using a vibrating tube densimeter. The speed of sound was here reported for the first time over $T=$ (303.15 to 353.15) K and $p=(0.1$ to 20.0) MPa, using an acoustic cell and a *Labview* interface designed for signal acquisition and processing. The experimental densities are very well correlated with the GMA EoS with an average relative deviation of 0.03%. The Paduszynki and Domanska predictive model was applied to predict the densities with an average absolute relative deviation of 1.7% which is within the expected uncertainty of the method. The volumetric derivative properties, that is, thermal expansivity and isothermal compressibility calculated from GMA EoS behave as expected relative to temperature and pressure variations. The experimental (upT) speed of sound data is well correlated with a rational function with an average absolute relative deviation of 0.08%. The density and speed of sound measurements were used to calculate the isentropic and the molar compressibilities in an extended range of pressures and temperatures. The molar compressibility is almost constant presenting a variation of less than 0.7 % over the considered ranges of temperature and pressure.

Acknowledgments

This work was developed in the scope of the project CICECO - Aveiro Institute of Materials, POCI-01-0145-FEDER-007679 (Ref. FCT UID/CTM/50011/2013), financed by national funds through the FCT/MEC and co-financed by FEDER under the PT2020 Partnership Agreement. P. J. Carvalho acknowledges FCT for a contract under the Investigador FCT 2015, contract number IF/00758/2015. S. Mattedi acknowledges the financial support from CNPq (grant N° 306640/2016-3).

Appendix A. Supplementary Information

Supplementary data associated with this article can be found, in the online version, at ...

References

- [1] D.F. Kennedy, C.J. Drummond, Large aggregated ions found in some protic ionic liquids, *J. Phys. Chem. B* 113 (2009) 5690.
- [2] J. Pernak, I. Goc, I. Mirska, Anti-microbial activities of protic ionic liquids with lactate anion, *Green Chem.* 6 (2004) 323–329.
- [3] R.V. Hangarge, D.V. Jarikote, M.S. Shingare, Knoevenagel condensation reactions in an ionic liquid *Green Chem.* 4 (2002) 266–268.
- [4] K.K. Laali, V.J. Gettwert, Electrophilic nitration of aromatics in ionic liquid solvents, *J. Org. Chem.* 66 (2001) 35–40.

- [5] Y. Hu, J. Chen, Z.G. Le, Q.G. Zheng, Organic reactions in ionic liquids: ionic liquids ethylammonium nitrate promoted Knoevenagel condensation of aromatic aldehydes with active methylene compounds, *Synth. Commun.* 35 (2005) 739–744.
- [6] C.F. Poole, Chromatographic and spectroscopic methods for the determination of solvent properties of room temperature ionic liquids, *J. Chromatogr. A* 1037 (2004) 49–82.
- [7] M.A.B.H. Susan, A. Noda, S. Mitsushima, M. Watanabe, Brønsted acid–base ionic liquids and their use as new materials for anhydrous proton conductors, *Chem. Commun.* 8 (2003) 938–939.
- [8] M.J. Earle, N.V. Plechkova, K.R. Seddon, Green synthesis of biodiesel using ionic liquids, *Pure Appl. Chem.* 81 (2009) 2045–2057.
- [9] J.C. Galvez-Ruiz, G. Holl, K. Karaghiosoff, T.M. Klapotke, K. Lohnwitz, P. Mayer, H. Noth, K. Polborn, C.J. Rohbogner, M. Suter, J.J. Weigand, Derivatives of 1,5-Diamino-1*H*-tetrazole: A new family of energetic heterocyclic-based salts, *Inorg. Chem.* 44 (2005) 4237–4253.
- [10] M. Picquet, I. Tkatchenko, I. Tommasi, P. Wasserscheid, J. Zimmermann, Ionic liquids, synthesis and utilization of protic imidazolium salts in homogeneous catalysis, *J. Adv. Synth. Catal.* 345 (2003) 959–962.
- [11] R.B. Trusler, Ethanolamine soaps, *Ind. Eng. Chem.* 21 (1929) 685–687.
- [12] S. Zhu, M. Heppenstall-Butler, M.F. Butler, P.D.A. Pudney, D. Ferdinando, K.J. Mutch, Acid soap and phase behaviour of stearic acid and triethanolamine stearate, *J. Phys. Chem. B* 109 (2005) 11753–11761.
- [13] S. Zhu, P.D.A. Pudney, M. Heppenstall-Butler, M.F. Butler, D. Ferdinando, M. Kirkland, Interaction of the acid soap of triethanolamine stearate and stearic acid with water, *J. Phys. Chem. B* 111 (2007) 1016–1024.

- [14] P.D.A. Pudney, K.J. Mutch, S.P. Zhu, Characterising the phase behaviour of stearic acid and its triethanolamine soap and acid-soap by infrared spectroscopy, *Phys. Chem. Chem. Phys.* 11 (2009) 5010-5018.
- [15] N.E. Meyer, Monoethanolamine oleate: a new chemical for the obliteration of varicose veins, *Am. J. Surg.* 40 (1938) 628-629.
- [16] K. Yamamoto, H. Sakaguchi, H. Anai, T. Tanaka, K. Morimoto, K. Kichikawa, H. Uchida, Sclerotherapy for simple cysts with use of ethanolamine oleate: preliminary experience, *Cardiovascular Intervent. Radiol.* 28 (2005) 751-755.
- [17] M.G. Kiripolsky, More on ethanolamine oleate as a vascular sclerosant, *Dermatol. Surg.* 36 (2010) 1153-1154.
- [18] C.C. Gomes, R.S. Gomez, M.A. do Carmo, W.H. Castro, A. Gala-Garcia, R.A. Mesquita, Mucosal varicosities: case report treated with monoethanolamine oleate, *Medicina oral, patologia oral y cirugia bucal* 11 (2006) E44-46.
- [19] K.A. Kurnia, C.D. Wilfred, T. Murugesan, Thermophysical properties of hydroxyl ammonium ionic liquids, *J. Chem. Thermodyn.* 41 (2009) 517-521.
- [20] M. Iglesias, R. Gonzalez-Olmos, I. Cota, F. Medina, Brønsted ionic liquids: Study of physico-chemical properties and catalytic activity in aldol condensations, *J. Chem. Eng. Data* 162 (2010) 802-808.
- [21] X. Wang, C. Ohlin, Q. Lu, Z. Fei, J. Hu, P.J. Dyson, Cytotoxicity of ionic liquids and precursor compounds towards human cell line HeLa, *Green Chem.* 9 (2007) 9, 1191-1197.
- [22] M.V.S. Oliveira, B.T. Vidal, C.M. Mel, R.C.M. de Miranda, C.M.F. Soares, J.A.P. Coutinho, S.P.M. Ventura, S. Mattedi, A.S. Lima, (Eco)toxicity and biodegradability of protic ionic liquids, *Chemosphere* 147 (2016) 460-466.

- [23] K.A. Kurnia, M.M. Taib, M.I.A. Mutalib, Densities, refractive indices and excess molar volumes for binary mixtures of protic ionic liquids with methanol at $T = 293.15$ to 313.15 K, *J. Mol. Liq.* 159 (2011) 211–219.
- [24] V.H. Alvarez, N. Dosil, R. Gonzalez-Cabaleiro, S. Mattedi, M. Martin-Pastor, M. Iglesias, J.M. Navaza, Bronsted ionic liquids for sustainable processes: synthesis and physical properties *J. Chem. Eng. Data* 55 (2010) 625–632.
- [25] A. Pinkert, K.L. Ang, K.N. Marsh, S. Pang, Density, viscosity and electrical conductivity of protic alkanolammonium ionic liquids, *Phys. Chem. Chem. Phys.* 13 (2011) 5136–5143.
- [26] N.M.C. Talavera-Prieto, A.G.M. Ferreira, P.N. Simões, P.J. Carvalho, S. Mattedi, J.A.P. Coutinho, Thermophysical characterization of N-methyl-2-hydroxyethylammonium carboxylate ionic liquids, *J. Chem. Thermodyn.* 68 (2014) 221–234.
- [27] Y. Li, E.J.P. Figueiredo, M.J.S.F. Santos, J.B. Santos, N.M.C. Talavera-Prieto, P.J. Carvalho, A.G.M. Ferreira, S. Mattedi, Volumetric and acoustical properties of aqueous mixtures of N-methyl-2-hydroxyethylammonium propionate at $T = (298.15$ to $333.15)$ K, *J. Chem. Thermodyn.* 88 (2015) 44–60.
- [28] Y. Li, E.J.P. Figueiredo, M.J.S.F. Santos, J.B. Santos, N.M.C. Talavera-Prieto, P.J. Carvalho, A.G.M. Ferreira, S. Mattedi, Volumetric and acoustical properties of aqueous mixtures of N-methyl-2-hydroxyethylammonium butyrate and N-methyl-2-hydroxyethylammonium pentanoate at $T = (298.15$ to $333.15)$ K, *J. Chem. Thermodyn.* 97 (2016) 191–205.
- [29] E.K. Goharshadi, A. Morsali, M. Abbaspour, New regularities and an equation of state for liquids, *Fluid Phase Equilib.* 230 (2005) 170–175.
- [30] R. Gardas, J. Coutinho, Extension of the Ye and Shreeve group contribution method for density estimation of ionic liquids in a wide range of temperatures and pressures, *Fluid Phase Equilib.* 263 (2008) 26–32.

- [31] K. Padászyński, U. Domańska, A new group contribution method for prediction of density of pure ionic liquids over a wide range of temperature and pressure, *Ind. Eng. Chem. Res.* 51 (2012) 591–604.
- [32] A. Kazakov, J.W. Magee, R.D. Chirico, V. Diky, C.D. Muzny, K. Kroenlein, M. Frenkel, NIST Standard Reference Database 147: NIST Ionic Liquids Database – (ILThermo)”, Version 2.0, Gaithersburg, MD: National Institute of Standards and Technology. Available at: <http://ilthermo.boulder.nist.gov>. Accessed November, 2017.
- [33] V.H. Alvarez, S. Mattedi, M. Martin-Pastor, M. Aznar, M. Iglesias, Thermophysical properties of binary mixtures of {ionic liquid 2-hydroxy ethylammonium acetate + (water, methanol, or ethanol)}, *J. Chem. Thermodyn.* 43 (2011) 997–1010.
- [34] I. Cota, R. Gonzalez-Olmos, M. Iglesias, F. Medina, New short aliphatic chain ionic liquids: synthesis, physical properties, and catalytic activity in aldol condensations, *J Phys Chem B.* 111 (2007) 12468–12477.
- [35] K.J. Wu, Q.L. Chen, C.H. He, Speed of sound of ionic liquids: database, estimation, and its application for thermal conductivity Prediction, *AIChE J.* 60 (2014) 1120–1131.
- [36] I.M.S. Lampreia, C.A. Nieto De Castro, A new and reliable calibration method for vibrating tube densimeters over wide ranges of temperature and pressure, *J. Chem. Thermodyn.* 43 (2011) 537–545.
- [37] A.G. M. Ferreira, J.B. Santos, M.J. Santos, A.T.G. Portugal, Speed of sound in pure fatty acid methyl esters and biodiesel fuels, *Fuel* 116 (2014) 242-254.
- [38] Thermophysical Properties of Fluid Systems - the NIST WebBook. <http://webook.nist.gov/chemistry/fluid> (accessed February, 2016).
- [39] R. Gomes de Azevedo, J. Szydłowski, P. Pires, J. Esperanca, H. Guedes and L. Rebelo, A novel non-intrusive microcell for sound-speed measurements in liquids. Speed of sound and thermodynamic properties of 2-propanone at pressures up to 160 MPa, *J. Chem. Thermodyn.* 36 (2004) 211-222.

- [40] E.K. Goharshadi, M. Moosavi, Thermodynamic properties of some ionic liquids using a simple equation of state. *J Mol Liq.* 142 (2008) 41–44.
- [41] M. R. J. Dack, The importance of solvent internal pressure and cohesion to solution phenomena, *Chem. Soc. Rev.* 4 (1975) 211-229.
- [42] I. A. Wiehe, E. B. Bagley, Estimation of dispersion and hydrogen bonding energies in liquids, *AIChE J.* 13 (1967) 836-838.
- [43] J.E.S.J. Reid, F. Agapito, C.E.S. Bernardes, F. Martins, A.J. Walker, S. Shimizu, M.E. Minas da Piedade, Structure–property relationships in protic ionic liquids: a thermochemical study, *Phys. Chem. Chem. Phys.* 19 (2017) 19928-199936.
- [44] V. Majer, V. Svoboda, Enthalpies of vaporization of organic compounds: a critical review and data compilation, Blackwell Scientific Publications, Oxford, 1985.
- [45] NIST Chemistry WebBook - the NIST WebBook. <http://webbook.nist.gov/cgi/> (accessed February 2016).
- [46] V. N. Kartsev, M. N. Rodnikova, I. Bartel, S. N. Shtykov, The temperature dependence of internal pressure in liquids, *Russian J. Phys. Chem.* 76 (2002) 1016 -1018.
- [47] V. N. Kartsev, To the understanding of the structural sensitivity of the temperature coefficient of internal pressure, *J. Struct. Chem.* 45 (2004) 832-837.
- [48] D.N.R. Thummuru, B.S. Mallik, Structure and dynamics of hydroxyl-functionalized protic ammonium carboxylate ionic liquids, 121 (2017) *J. Phys. Chem. A* 8097-8107.
- [49] E. V. Ivanov and V. K. Abrosimov, Relationship between the internal pressure and cohesive energy density of a liquid nonelectrolyte. Consequences of application of Dack's concept, *J. Structural Chemistry* 46 (2005) 856-861.

[50] T. Singh, A. Kumar, Static dielectric constant of room temperature ionic liquids: internal pressure and cohesive energy density approach, *J. Phys. Chem. B* 112 (2008) 12968–12972.

[51] C. Ye, J.M. Shreeve, Rapid and accurate estimation of densities of room-temperature ionic liquids and salts, *J. Phys. Chem. A* 111 (2007) 1456–1461.

[52] J. O. Valderrama, R. E. Rojas, Critical properties of ionic liquids. Revisited, *Ind. Eng. Chem. Res.* 48 (2009) 6890–6900.

[53] Y. Wada, On the relation between compressibility and molal volume of organic liquids, *J. Phys. Soc. Jpn.* 4 (1949) 280–283.

Figure Captions

Figure 1. Schematic apparatus – 1: High pressure valves; 2: ultrasound cell; 3: signal generator; 4: NI-PCI data acquisition board (PCIe-9852); 5: PC; 6: buffer; 7: pressure generator (model 50-6-15, High Pressure Co); 8: pressure transducer (Keller, Mano 2000 LEO 2).

Figure 2. Experimental density for [2-HEA][Pr]. The lines represent the fitting with GMA EoS. Δ , 298.15 K; ∇ , 303.15 K; \circ , 313.15 K; \square , 323.15 K; \diamond , 333.15 K; +, 343.15 K.

Figure 3. Density as function of temperature for the [2-HEA][Pr], at atmospheric pressure. The open symbols refer to the data reported here and the values reported by Kurnia *et al.* [23].

Figure 4. Isotherms of $(2z-1)V_m^3$ versus the molar density (ρ_m) for [2-HEA][Pr] calculated from GMA EoS. Δ , 298.15 K; ∇ , 303.15K; \circ , 313.15 K; \square , 323.15 K; \diamond , 333.15 K; +, 343.15 K. Symbols represent experimental *PVT* data and the full lines are for the GMA EoS.

Figure 5. Relative density deviations between the experimental density (ρ) and that calculated with the GMA EoS (ρ_{cal}). Δ , 298.15 K; ∇ , 303.15K; \circ , 313.15 K; \square , 323.15 K; \diamond , 333.15 K; $+$, 343.15 K.

Figure 6. Thermal expansivity of [2-HEA][Pr] as a function of pressure and temperature. Δ , 298.15 K; ∇ , 303.15K; \circ , 313.15 K; \square , 323.15 K; \diamond , 333.15 K; $+$, 343.15 K. Symbols and lines represent calculations from GMA EoS.

Fig 7. Isothermal compressibility of [2-HEA][Pr] as function of pressure and temperature from GMA EoS. Δ , 298.15 K; ∇ , 303.15K; \circ , 313.15 K; \square , 323.15 K; \diamond , 333.15 K; $+$, 343.15 K. Symbols and lines represent calculations from GMA EoS.

Figure 8. Internal pressure of [2-HEA][Pr] as function of temperature calculated from GMA EoS. \circ , $p=0.1$ MPa; \square , $p=35$ MPa; \bullet , CED at $T = 298.15$ K and $p=0.1$ MPa. Symbols and lines represent calculations from GMA EoS.

Figure 9. Relative density deviations between the calculated values with GC GCM (a) and PD GCM (b) models (ρ_{cal}) and the experimental values of this work (ρ). Δ , 298.15 K; ∇ , 303.15K; \circ , 313.15 K; \square , 323.15 K; \diamond , 333.15 K; $+$, 343.15 K.

Figure 10. Sound speed of [2-HEA][Pr] as function of pressure and temperature. Experimental data: Δ , 298.15 K; ∇ , 303.15 K; \circ , 313.15 K; \square , 323.15 K; \diamond , 333.15 K; $+$, 343.15 K. The lines represent the fitting with Eq. (21).

Figure 11. Relative deviations of sound speed between the experimental (u) values and those calculated using Eq. (21) (u_{cal}). Δ , 303.15 K; ∇ , 313.15 K; \circ , 323.15 K; \square , 333.15 K; \diamond , 343.15 K; $+$, 353.15. The dashed lines represent the limits for $\%AARD_u = \pm 0.09\%$ (see Table 6).

Figure 12. Speed of sound of [2-HEA][F], [2-HEA][Ac], [2-HEA][Pr] and [2-HEA][Pe] as a function of temperature. Experimental values: $+$, [2HEA][F] [33]; Δ , [2HEA][Ac] [32]; \times , [2HEA][Pe] [20]; \circ , [2HEA][Pr] this work. Solid line refers to predictive Wu *et al.* [34] method.

Figure 13. Isentropic compressibility of [2-HEA][Pr] as function of temperature and pressure. Experimental values: ∇ , 303.15K; \circ , 313.15 K; \square , 323.15 K; \diamond , 333.15 K; $+$, 343.15 K. Lines refer to the calculations from combined GMA EoS and Eq. (25) (dashed line is relative to 298.15K).

ACCEPTED MANUSCRIPT

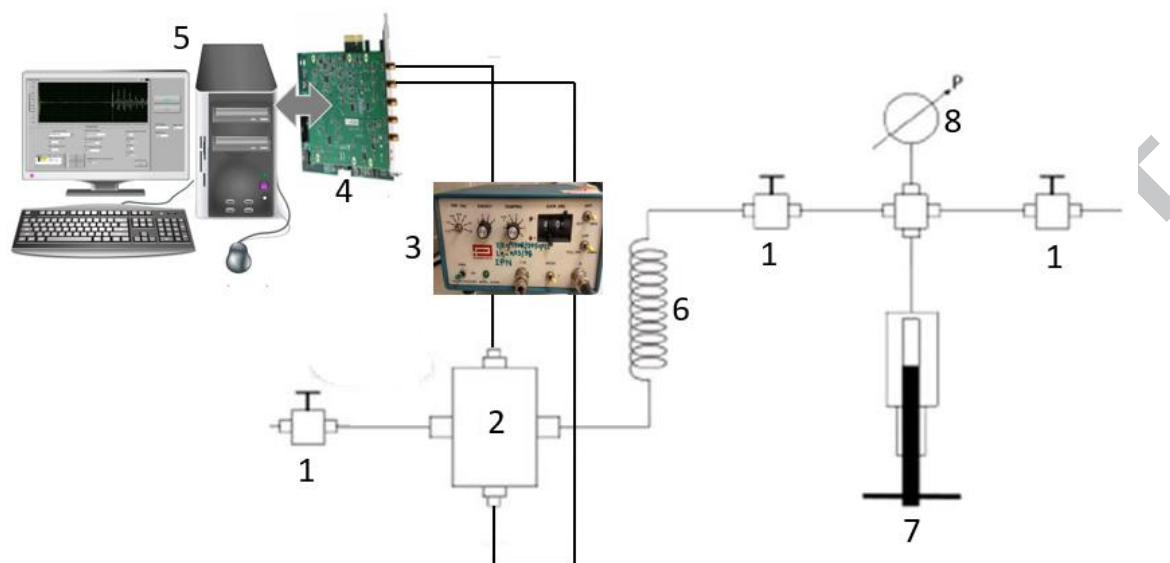


Fig. 1. Schematic apparatus – 1: High pressure valves; 2: ultrasound cell; 3: signal generator; 4: NI-PCI data acquisition board (PCIe-9852); 5: PC; 6: buffer; 7: pressure generator (model 50-6-15, High Pressure Co); 8: pressure transducer (Keller, Mano 2000 LEO 2).

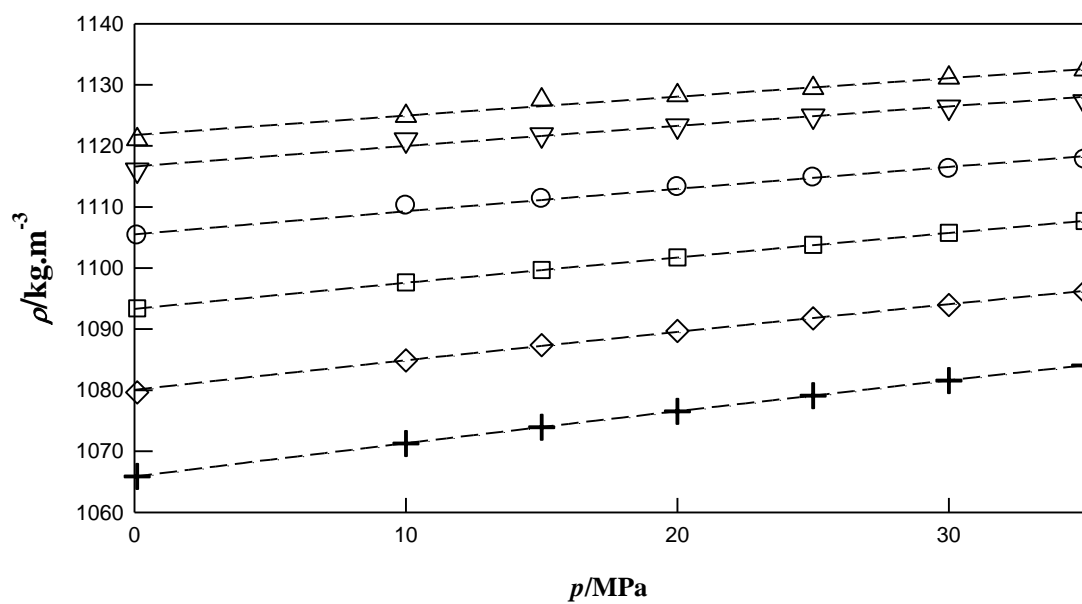


Fig. 2. Experimental density for [2-HEA][Pr]. Δ , 298.15 K; ∇ , 303.15 K; \circ , 313.15 K; \square , 323.15 K; \diamond , 333.15 K; $+$, 343.15 K. The lines represent the fitting with GMA EoS.

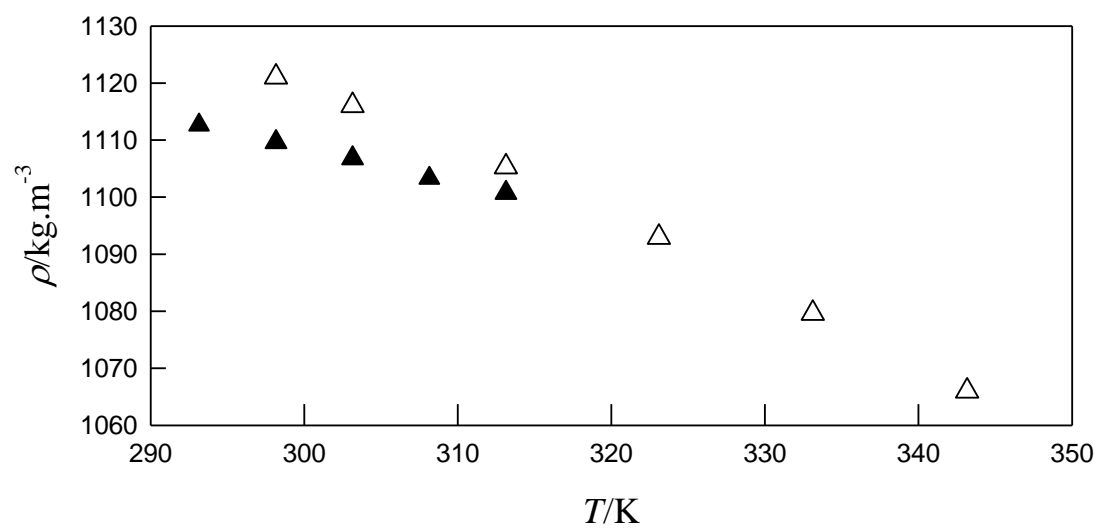


Fig. 3. Density as function of temperature for the [2-HEA][Pr], at atmospheric pressure. The open symbols refer to the data reported here and the closed ones those reported by Kurnia *et al.* [23].

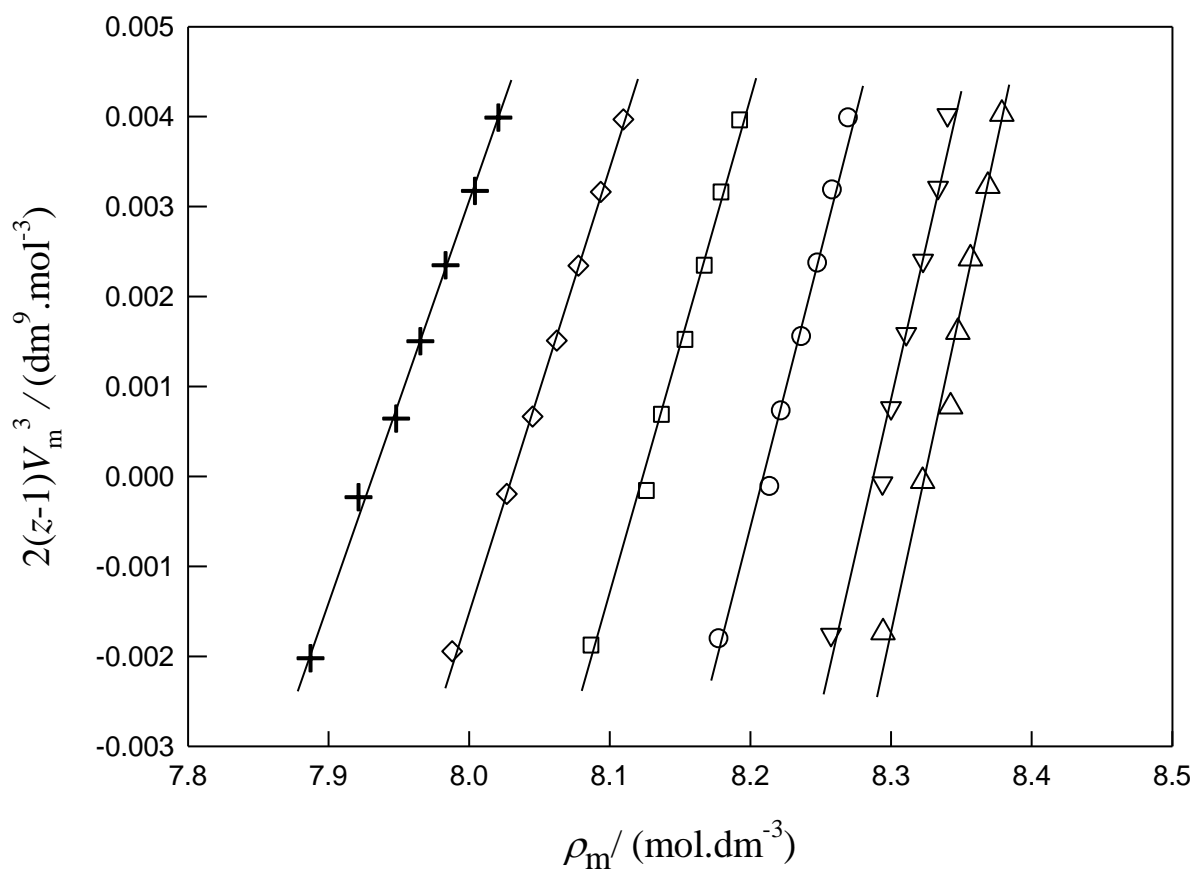


Fig. 4. Isotherms of $(2z-1)V_m^3$ versus the molar density (ρ_m) for [2-HEA][Pr] calculated from GMA EoS. Δ , 298.15 K; ∇ , 303.15K; \circ , 313.15 K; \square , 323.15 K; \diamond , 333.15 K; $+$, 343.15 K. The full lines represent the GMA EoS.

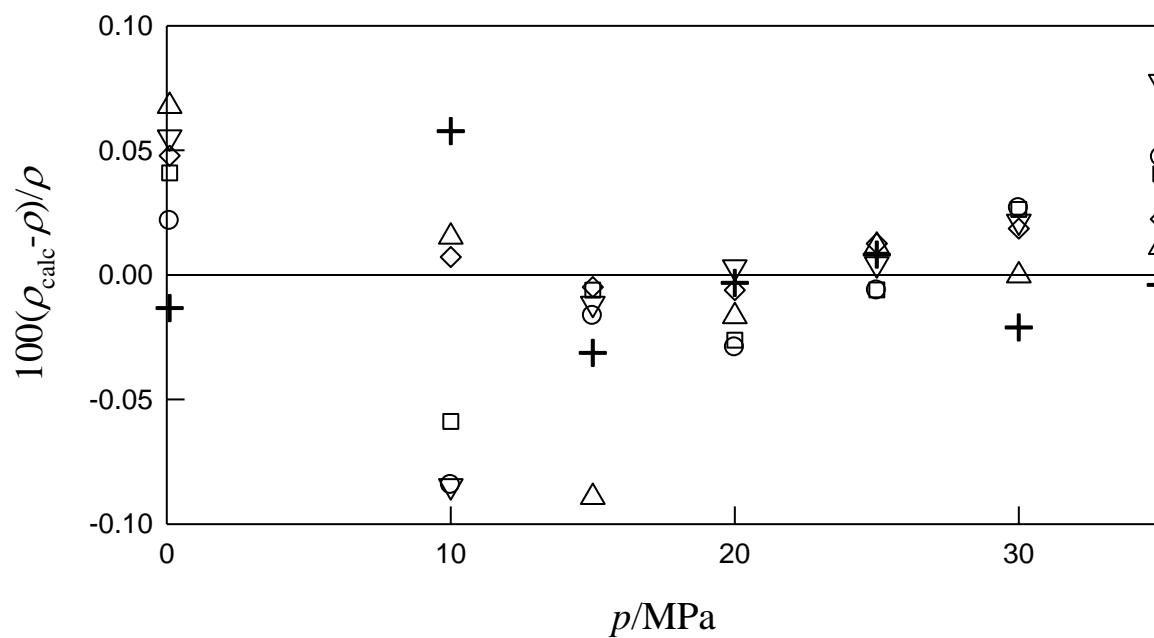


Fig. 5. Relative density deviations between the experimental density (ρ) and that calculated with the GMA EoS (ρ_{calc}). Δ , 298.15 K; ∇ , 303.15K; \circ , 313.15 K; \square , 323.15 K; \diamond , 333.15 K; $+$, 343.15 K

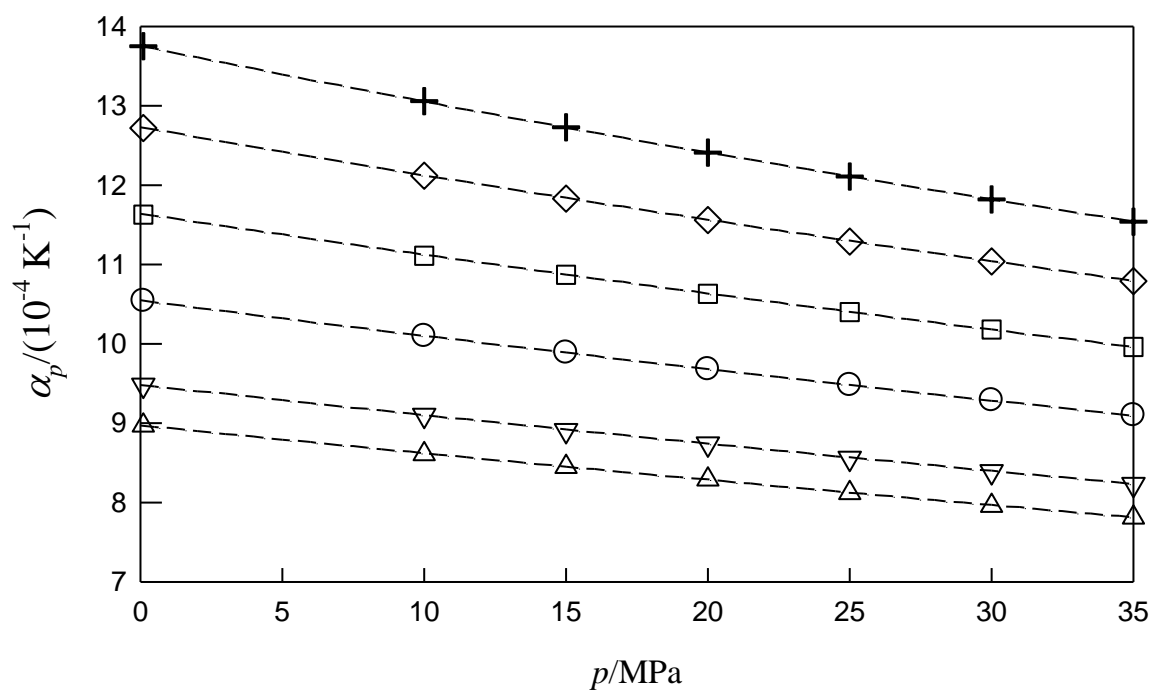


Fig. 6. Thermal expansivity of [2-HEA][Pr] as a function of pressure and temperature. Δ , 298.15 K; ∇ , 303.15 K; \circ , 313.15 K; \square , 323.15 K; \diamond , 333.15 K; $+$, 343.15 K. Symbols and lines represent calculations from GMA EoS.

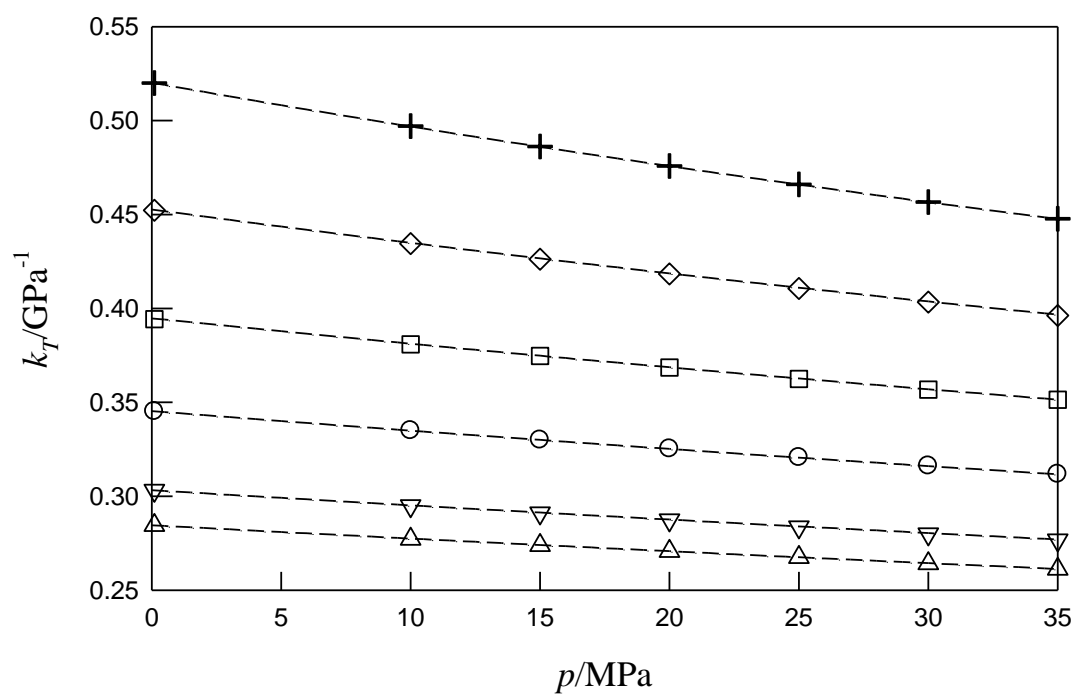


Fig 7. Isothermal compressibility of [2-HEA][Pr] as function of pressure and temperature from GMA EoS. Δ , 298.15 K; ∇ , 303.15K; \circ , 313.15 K; \square , 323.15 K; \diamond , 333.15 K; $+$, 343.15 K. Symbols and lines represent calculations from GMA EoS.

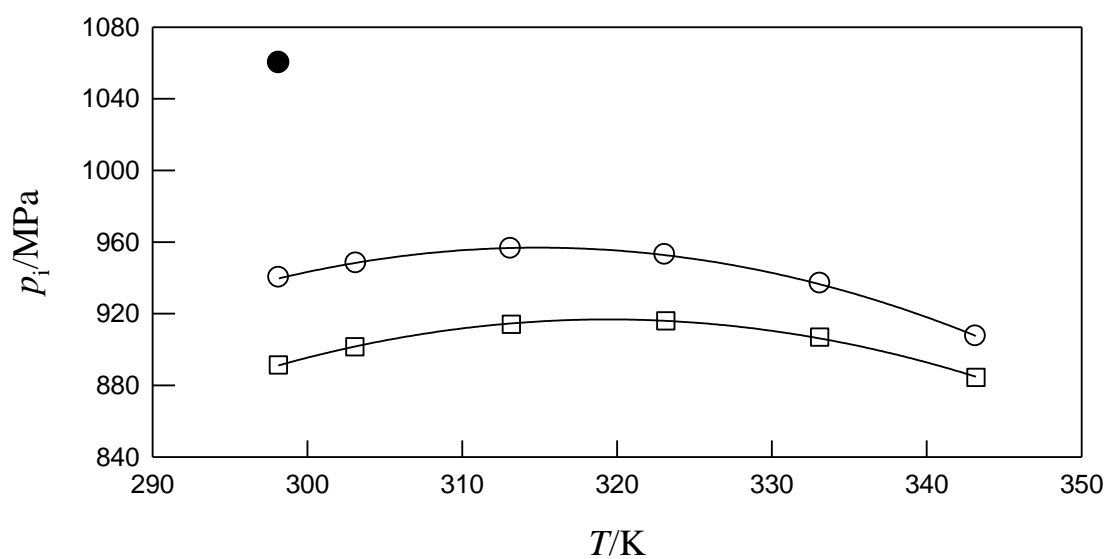


Fig. 8. Internal pressure of [2-HEA][Pr] as function of temperature calculated from GMA EoS. \circ , $p=0.1$ MPa; \square , $p=35$ MPa; \bullet , CED at $T = 298.15$ K and $p=0.1$ MPa. Symbols and lines represent calculations from GMA EoS.

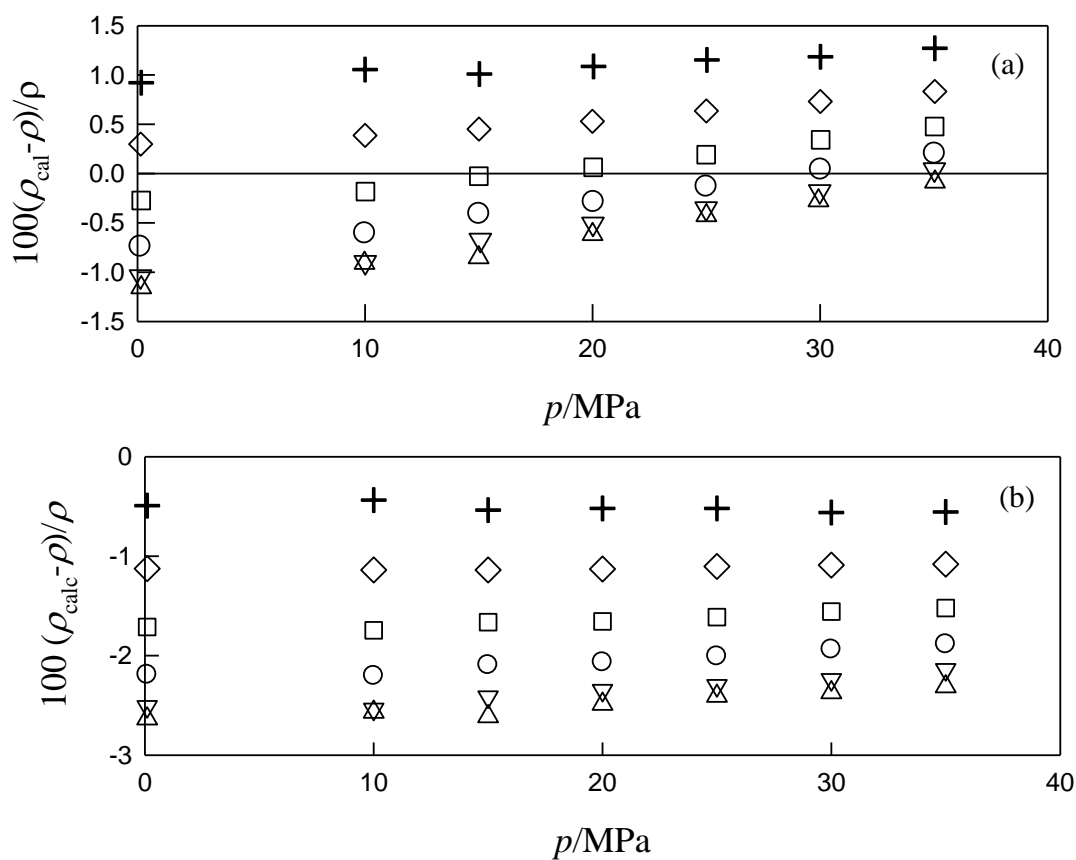


Fig. 9. Relative density deviations between the calculated values with GC GCM (a) and PD GCM (b) models (ρ_{cal}) and the experimental values of this work (ρ). Δ , 298.15 K; ∇ , 303.15K; \circ , 313.15 K; \square , 323.15 K; \diamond , 333.15 K; $+$, 343.15 K.

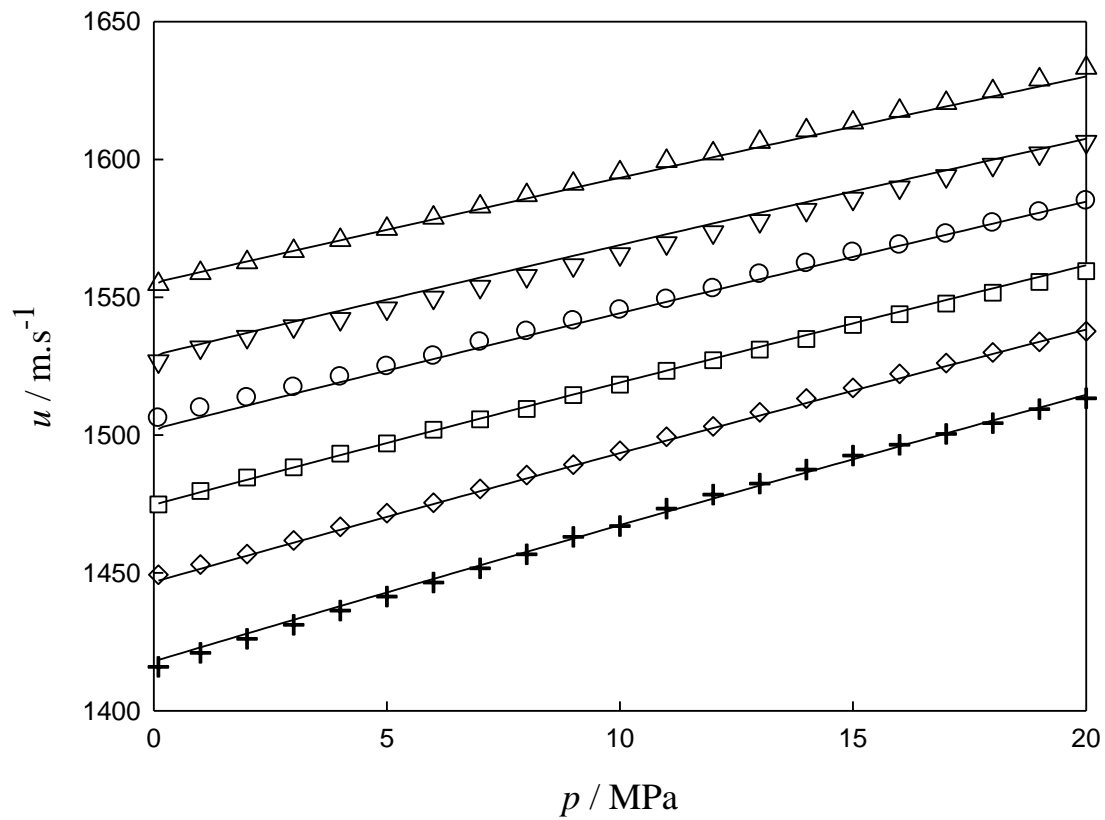


Fig. 10. Sound speed of [2-HEA][Pr] as function of pressure and temperature. Experimental data: Δ , 303.15 K; ∇ , 313.15 K; \circ , 323.15 K; \square , 333.15 K; \diamond , 343.15 K; +, 353.15 K. The lines represent the fitting with Eq. (21).

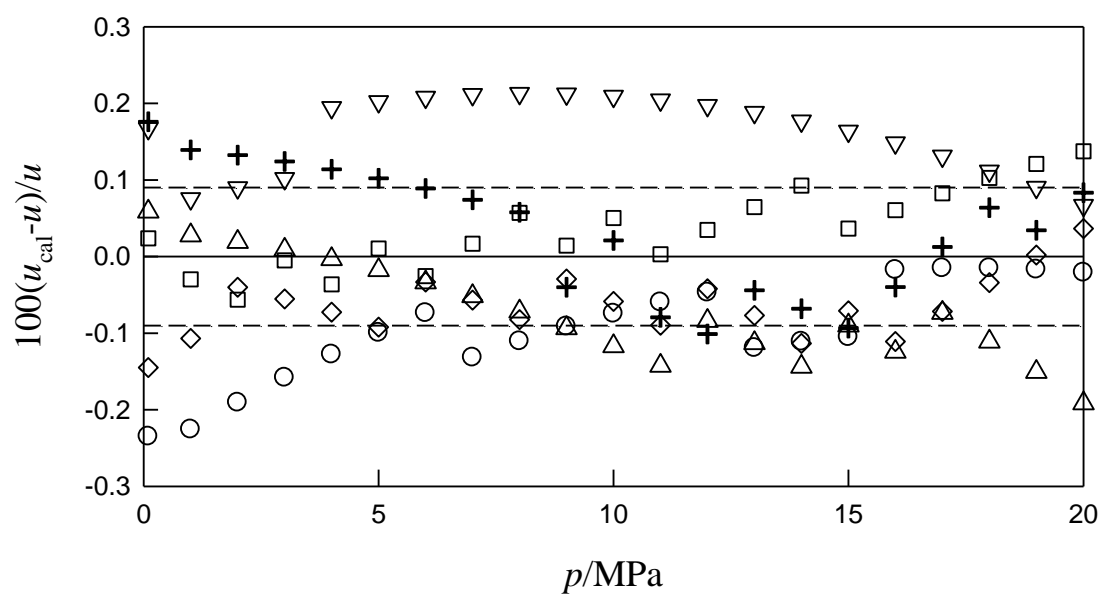


Fig. 11. Relative deviations of sound speed between the experimental (u) values and those calculated using Eq. (21) (u_{cal}). Δ , 303.15 K; ∇ , 313.15 K; \circ , 323.15 K; \square , 333.15 K; \diamond , 343.15 K; $+$, 353.15 K. The dashed lines represent the limits for $\%AARD_u = \pm 0.09\%$ (see Table 6).

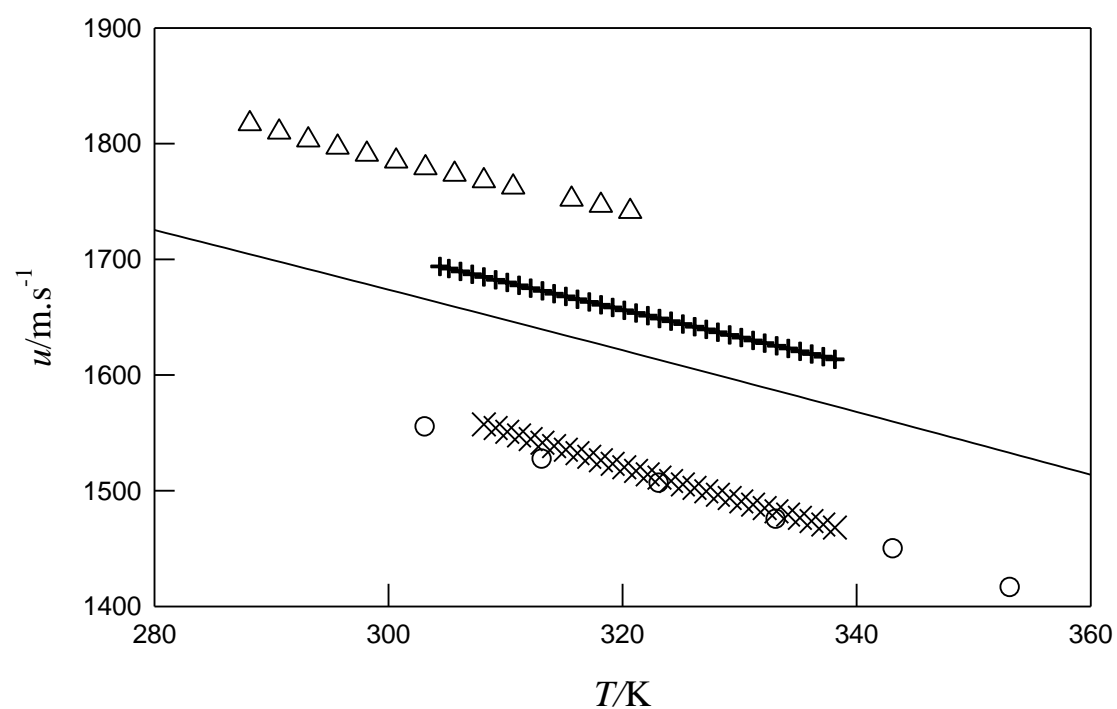


Fig. 12. Speed of sound of [2-HEA][F], [2-HEA][Ac], [2-HEA][Pr] and [2-HEA][Pe] as a function of temperature. Experimental values: +, [2-HEA][F] [33]; Δ , [2-HEA][Ac] [32]; \times , [2-HEA][Pe] [20]; \circ , [2-HEA][Pr] this work. Solid line refers to predictive Wu *et al.* [34] method.

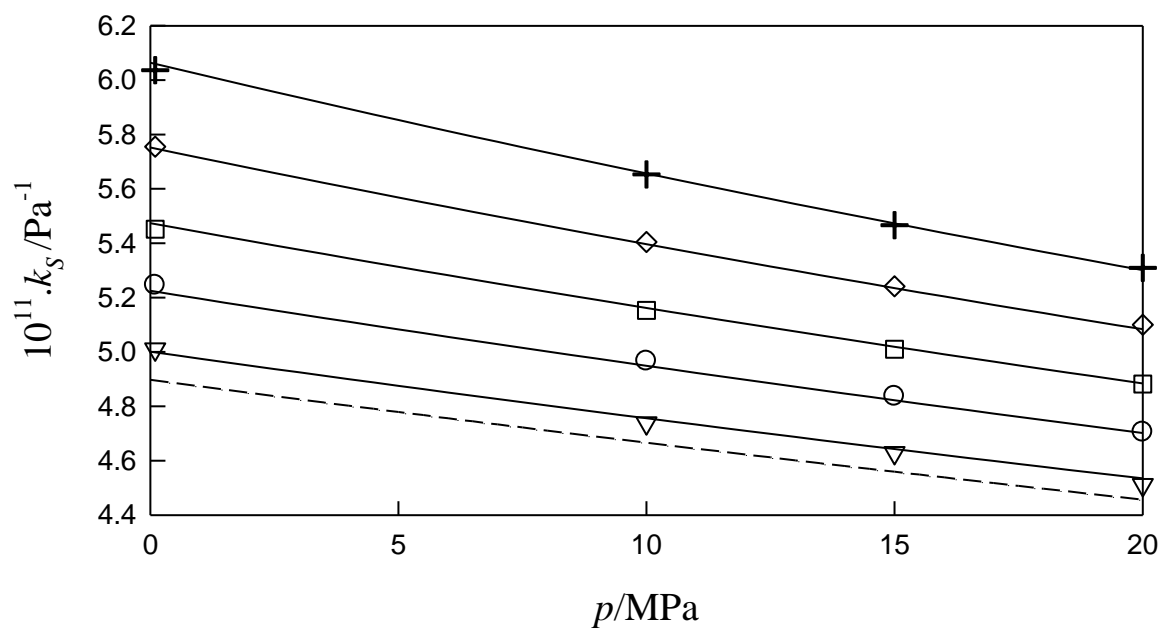


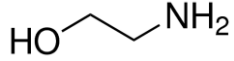
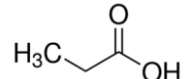
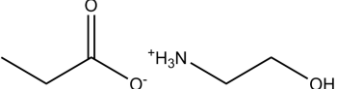
Fig. 13. Isentropic compressibility of [2-HEA][Pr] as function of temperature and pressure. Experimental values: ∇ , 303.15K; \circ , 313.15 K; \square , 323.15 K; \diamond , 333.15 K; +, 343.15 K. Lines refer to the calculations from combined GMA EoS and Eq. (25) (dashed line is relative to 298.15K).

Table 1

Chemical structure, compound description, CAS Number, molecular weight, water mass fraction content, mass fraction purity and supplier of the studied compounds.

Properties of the materials used in the study.

Chemical samples description.

Compound	Chemical structure
Ethanolamine (CAS: 141-43-5 ; Mw = 61.08 g mol ⁻¹ ; wt% ≥ 98% ^a) acquired from Sigma-Aldrich	
Propanoic Acid (CAS: 79-09-4 ; Mw = 74.08 g mol ⁻¹ ; wt% ≥ 98% ^a) acquired from Sigma-Aldrich	
Water (CAS: 7732-18-5 ; Mw = 18.02 g mol ⁻¹ ; wt% ≥ 98% ^a) obtained from Milli-Q	
Toluene (CAS: 108-88-3 ; Mw = 92.14 g mol ⁻¹ ; wt% ≥ 99.999% ^a) acquired from Fisher Scientific	
2-hydroxyethylammonium propionate ([2-HEA][Pr]) (Mw = 135.16 g mol ⁻¹ ; H ₂ O wt < 100 ppm ; wt% ≥ 98% ^b)	

^aas reported by the supplier. ^bafter moderate temperature and vacuum procedure.

Table 2

Calibration constants C_i of Eq. (1) fitted to experimental speed of sound of water and toluene with 95% confidence limits and statistical indicators.

Parameter	Value	Parameter	Value
$C_1 / \text{s} \cdot \text{m}^{-1}$	-0.00324269	C_7 / m^{-1}	300.9724
$C_2 / \text{s} \cdot \text{m}^{-1} \cdot \text{K}^{-1}$	2.02098×10^{-5}	$C_8 / \text{m}^{-1} \cdot \text{K}^{-1}$	-1.55832
$C_3 / \text{s} \cdot \text{m}^{-1} \cdot \text{K}^{-2}$	-3.19176×10^{-8}	$C_9 / \text{m}^{-1} \cdot \text{K}^{-2}$	2.45322×10^{-3}
$C_4 / \text{s} \cdot \text{m}^{-1} \cdot \text{MPa}^{-1}$	1.48993×10^{-4}	$C_{10} / \text{m}^{-1} \cdot \text{MPa}^{-1}$	-11.6543
$C_5 / \text{s} \cdot \text{m}^{-1} \cdot \text{K}^{-1} \cdot \text{MPa}^{-1}$	-9.52215×10^{-7}	$C_{11} / \text{m}^{-1} \cdot \text{K}^{-1} \cdot \text{MPa}^{-1}$	7.44899×10^{-2}
$C_6 / \text{s} \cdot \text{m}^{-1} \cdot \text{K}^{-2} \cdot \text{MPa}^{-1}$	1.52256×10^{-9}	$C_{12} / \text{m}^{-1} \cdot \text{K}^{-2} \cdot \text{MPa}^{-1}$	-1.19134×10^{-4}
$\sigma_{1/u} / \text{s} \cdot \text{m}^{-1}$	2.717×10^{-7}	$\sigma_u / \text{m} \cdot \text{s}^{-1}$	0.63
r^2	1.0000	%AARD _u	0.032

Table 3

Experimental density data (ρ) for [2-HEA][Pr] as a function of temperature (T) and pressure (p).

p/MPa	T/K	$\rho/\text{kg}\cdot\text{m}^{-3}$	T/K	$\rho/\text{kg}\cdot\text{m}^{-3}$	T/K	$\rho/\text{kg}\cdot\text{m}^{-3}$	T/K	$\rho/\text{kg}\cdot\text{m}^{-3}$	T/K	$\rho/\text{kg}\cdot\text{m}^{-3}$	T/K	$\rho/\text{kg}\cdot\text{m}^{-3}$
0.1	298.16	1121.1	303.15	1116.0	313.14	1105.3	323.10	1093.0	333.12	1079.6	343.17	1066.0
10.0	298.08	1124.9	303.09	1121.0	313.17	1110.2	323.09	1098.3	333.09	1084.9	343.19	1070.6
15.0	298.11	1127.6	303.09	1121.8	313.16	1111.3	323.14	1099.7	333.09	1087.4	343.18	1074.3
20.0	298.15	1128.2	303.10	1123.3	313.18	1113.3	323.14	1102.0	333.10	1089.7	343.17	1076.6
25.0	298.15	1129.4	303.07	1124.9	313.19	1114.8	323.10	1103.9	333.09	1091.8	343.17	1079.0
30.0	298.10	1131.1	303.03	1126.3	313.18	1116.2	323.12	1105.5	333.09	1093.9	343.17	1081.8
35.0	298.13	1132.5	303.07	1127.2	313.17	1117.8	323.14	1107.3	333.08	1096.1	343.18	1084.1

Uncertainties are: $u(T) = \pm 0.02$ K, $u(p) = \pm 0.02$ MPa and $u_c(\rho) = \pm 0.45$ $\text{kg}\cdot\text{m}^{-3}$.

Table 4

Parameters A_0 - A_2 , and B_0 - B_2 of Eqs. (5) and (6), temperature and pressure ranges (T_{\min} , T_{\max} , p_{\min} , p_{\max}), standard deviation (σ) correlation coefficient (r^2) number of data points (N), and standard deviation on density (σ_ρ).

$M/\text{g}\cdot\text{mol}^{-1}$	135.16	p_{\min}/MPa	0.10
$A_0/\text{dm}^9\cdot\text{mol}^{-3}$	30.1331934	p_{\max}/MPa	35.0
$A_1/\text{MPa}\cdot\text{dm}^{12}\cdot\text{mol}^{-4}$	8.00712813	$\sigma/\text{dm}^9\cdot\text{mol}^{-3}$	2.12×10^{-4}
$A_2/\text{MPa}\cdot\text{dm}^{12}\cdot\text{mol}^{-4}\cdot\text{K}^{-1}$	-0.0177130	r^2	0.994
$B_0/\text{dm}^{12}\cdot\text{mol}^{-4}$	-3.3818027	$\sigma_\rho/\text{kg}\cdot\text{m}^{-3\text{ a}}$	0.45
$B_1/\text{MPa}\cdot\text{dm}^{15}\cdot\text{mol}^{-5}$	-0.8984098	N	42
$B_2/\text{MPa}\cdot\text{dm}^{15}\cdot\text{mol}^{-5}\cdot\text{K}^{-1}$	0.00199151	$\%AARD_\rho$	0.03
T_{\min}/K	298.08		
T_{\max}/K	343.19		

^a The standard deviation relative to the density is $\sigma_\rho = \left[\sum_{i=1}^N (\rho_{\text{calc}} - \rho)_i^2 / (N-6) \right]^{1/2}$ with $\sigma_\rho / (\text{kg}\cdot\text{m}^{-3})$. N is the number of data points, ρ_{calc} is the calculated value of density and ρ is the reported experimental value at the same temperature (and pressure).

Table 5

Experimental values of speed of sound (u) for [2-HEA][Pr] as a function of temperature (T) and pressure (p).

p /MPa	u (m·s ⁻¹) at T (K)					
	303.15	313.15	323.15	333.15	343.15	353.15
0.1	1554.7	1526.8	1506.1	1474.9	1449.3	1416.0
1.0	1558.7	1531.9	1509.8	1479.7	1453.0	1421.0
2.0	1562.7	1535.7	1513.6	1484.6	1456.8	1426.1
3.0	1566.7	1539.5	1517.3	1488.3	1461.8	1431.2
4.0	1570.7	1542.1	1521.1	1493.2	1466.7	1436.3
5.0	1574.7	1546.0	1524.9	1497.0	1471.7	1441.4
6.0	1578.8	1549.9	1528.7	1501.9	1475.5	1446.5
7.0	1582.9	1553.8	1533.8	1505.7	1480.5	1451.7
8.0	1587.0	1557.8	1537.6	1509.5	1485.5	1456.8
9.0	1591.1	1561.7	1541.5	1514.5	1489.3	1463.1
10.0	1595.2	1565.7	1545.4	1518.3	1494.3	1467.0
11.0	1599.4	1569.7	1549.2	1523.3	1499.4	1473.3
12.0	1602.1	1573.7	1553.2	1527.2	1503.2	1478.4
13.0	1606.3	1577.7	1558.4	1531.0	1508.2	1482.4
14.0	1610.5	1581.7	1562.3	1534.9	1513.3	1487.5
15.0	1613.3	1585.8	1566.3	1540.0	1517.2	1492.6
16.0	1617.6	1589.9	1568.9	1543.8	1522.2	1496.5
17.0	1620.4	1594.0	1572.9	1547.7	1526.1	1500.4
18.0	1624.6	1598.1	1576.9	1551.6	1530.0	1504.4
19.0	1628.9	1602.2	1581.0	1555.5	1533.8	1509.5
20.0	1633.2	1606.4	1585.0	1559.5	1537.7	1513.3

Uncertainties are: $u(T) = \pm 0.05$ K, $u(p) = \pm 0.02$ MPa and $u_c(u) = \pm 1.6$ m·s⁻¹.

Table 6

Parameters a_0 - a_3 , b_1 and b_2 of Eq. (21), temperature and pressure ranges (T_{\min} , T_{\max} , p_{\min} , p_{\max}), standard deviation (σ_u) correlation coefficient (r^2) number of data points (N) and average absolute relative deviation, %AARD.

$a_0 / \text{m}\cdot\text{s}^{-1}$	2243.811	p_{\min} / MPa	0.10
$a_1 / \text{m}\cdot\text{s}^{-1}\cdot\text{K}^{-1}$	-5.99823	p_{\max} / MPa	20.0
$a_2 / \text{m}\cdot\text{s}^{-1}\cdot\text{K}^{-2}$	3.41052×10^{-3}	r^2	0.9989
a_3 / K^{-1}	-1.73154×10^{-3}	$\sigma_u / \text{m}\cdot\text{s}^{-1}$	1.70
$b_1 / \text{m}\cdot\text{s}^{-1}\cdot\text{MPa}^{-1}$	3.19043	N_p	126
b_2 / MPa^{-1}	8.66638×10^{-4}	%AARD _u	0.09
T_{\min} / K	303.15		
T_{\max} / K	353.15		

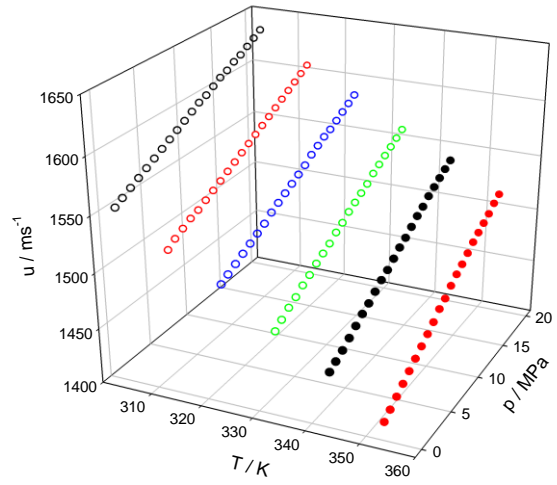
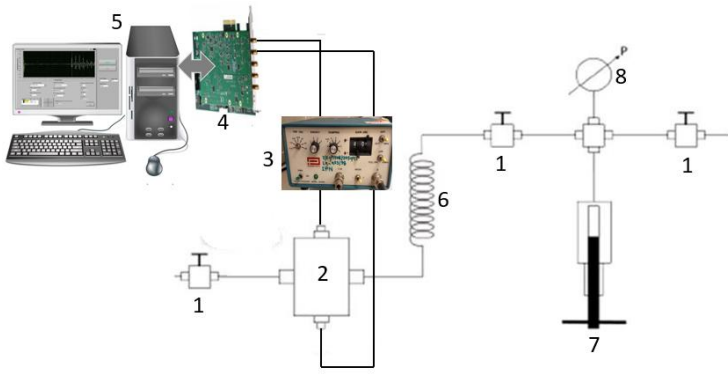
Table 7

Molar compressibility (k_m) of [2-HEA][Pr] as function of temperature and pressure. The mean molar compressibilities, $\langle k_m \rangle$, taken over pressure or temperature ranges, and corresponding standard deviations are presented.

p /MPa	$k_m 10^5 / \text{m}^3 \cdot \text{mol}^{-1} \cdot \text{Pa}^{1/7}$					$(\langle k_m \rangle, T)_p \pm \sigma$
	303.15 K	313.15 K	323.15 K	333.15 K	343.15 K	
0.1	3.586	3.597	3.618	3.634	3.656	3.618 ± 0.025
10.0	3.599	3.609	3.629	3.649	3.674	3.632 ± 0.027
15.0	3.608	3.620	3.639	3.657	3.679	3.641 ± 0.026
20.0	3.617	3.627	3.645	3.663	3.687	3.648 ± 0.025
$(\langle k_m \rangle, p)_T \pm \sigma$	3.602 ± 0.011	3.613 ± 0.011	3.633 ± 0.010	3.651 ± 0.011	3.674 ± 0.011	3.635 ± 0.026^a 3.635 ± 0.011^b
Total $\langle k_m \rangle \pm \sigma$	3.635 ± 0.028					

^a $\langle k_m \rangle$ for $(\langle k_m \rangle, T)_p$

^b $\langle k_m \rangle$ for $(\langle k_m \rangle, p)_T$.



ACCEPTED MANUSCRIPT

Highlights

- Density and speed of sound of 2-hydroxyethylammonium propionate ionic liquid are measured.
- Experimental pVT data were very well correlated with Goharshadi–Morsali–Abbaspour equation of state.
- Experimental pVT data were successfully described by predictive methods.
- Experimental speed of sound data is well correlated with a rational function.
- The molar compressibility is almost constant with temperature and pressure.